Journal of Hydrology: Regional Studies 66 (2026) 103551

Contents lists available at ScienceDirect

Journal of Hydrology: Regional Studies

journal homepage: www.elsevier.com/locate/ejrh

Compound coastal flooding in high-latitude Baltic Sea estuaries of Finland: Patterns, seasonality and trends

Tua Nylén *, Harri Tolvanen

Department of Geography and Geology, University of Turku, TURUN YLIOPISTO, FI-20014, Finland

A R T I C L E I N F O

Keywords:
Coastal flood
River flood
Seasonality
Land uplift
Baltic Sea
Peaks over threshold
Copula modelling

A B S T R A C T

Study region: Baltic Sea estuaries of Finland, 60–66° N.

Study focus: Joint sea level–streamflow peaks may cause severe and underestimated flood hazard in estuaries, and their likelihood is modified by climate change. Information is urgently needed on compound flood potential in the high-latitude estuaries, and its latitudinal, seasonal, and decadal variation. We address this by comparing sea level and streamflow data for 11 sites along the Finnish coast in 1971–2024.

New hydrological insights for the region: The co-variability between sea level and streamflow is low in northernmost Finland and highest in the south-west. Compound flood events are most frequent in south-west and their return periods increase northward and eastward towards the Baltic Sea gulfs. In the north, sea level and streamflow peaks are seasonally offset, occurring during autumn and winter, and during spring snowmelt season, respectively. Potentially, more joint peaks occur in the south because catchments often remain unfrozen and receive some of the precipitation as rain during the winter months. The hydrological winter is beginning increasingly late in the north, which may have led to more frequent compound flood events. While the inferred patterns are moderated by regional factors (Baltic Sea oceanography and climatology), we hypothesize that the compound flood probability in the high-latitude estuaries is impacted by the state of precipitation during the storm season, and therefore highly sensitive to the changing climate.

1. Introduction

Worldwide, floods are both the most widespread and the most financially costly natural disasters (Mishra et al., 2022; Rentschler et al., 2022). Coastal flood susceptibility is increasing globally due to accelerating sea level rise and intensifying storms creating storm surges, and higher-intensity rainfall events (Hinkel et al., 2014; Vousdoukas et al., 2018; Ward et al., 2018; Taherkhani et al., 2020; Nicholls et al., 2021). Also waves and (spring) tides together with snow melt and increased surface runoff and streamflow contribute to the flood events (e.g., Zscheischler et al., 2018; Couasnon et al., 2020; Nasr et al., 2021, Lewis et al., 2024). In some coastal regions land subsidence further increases the flood potential (Nicholls et al., 2021; Wu et al., 2024). In deltas and estuaries, the simultaneous peaks in sea level and streamflow may lead to extreme flood events, referred to as coastal compound flooding (Ward et al., 2018; Couasnon et al., 2020; Ghanbari et al., 2021). Low-lying estuarine coasts face highest flood hazard (e.g., Sangsefidi et al., 2023; Wu et al., 2024; Nasr et al., 2021), and densely populated coasts with expensive infrastructure have highest risk, in terms of loss of life, houses and infrastructure (Sebastian, 2022; Green et al., 2025).

* Corresponding author.
E-mail addresses: tua.nylen@utu.fi (T. Nylén), harri.tolvanen@utu.fi (H. Tolvanen).

https://doi.org/10.1016/j.ejrh.2026.103551
Received 30 January 2026; Received in revised form 6 April 2026; Accepted 16 May 2026
Available online 26 May 2026

Compound flood events may be caused by synoptic weather systems, leading to event occurrence that exceeds statistical independence (Seneviratne et al., 2012). They are often linked to advancing low-pressure systems (e.g., reviewed by Green et al., 2025), which are expected to become stronger and more frequent due to climate change (Little et al., 2023), making it essential to understand their behaviour. Most existing flood hazard models and maps treat sea level and streamflow as separate flood drivers, and may therefore underestimate the effects of their co-occurrence in estuaries (e.g., Ikeuchi et al., 2017; Couasnon et al., 2018; Zscheischler et al., 2018; Moftakhari et al., 2019; Serafin et al., 2019; de Ruiter et al., 2020; Ward et al., 2022; Fassert et al., 2023).

Prior research generally indicates that compound flooding is increasing particularly in the high latitudes (Wahl et al., 2015; Bevacqua et al., 2019, 2020; Lai et al., 2021). It has been suggested that the seasonal patterns in sea level and streamflow are important for the compound flooding hazard, and that recent changes in these patterns may lengthen the so-called compound flood season at least in northern Europe (Heinrich et al., 2023 based on simulated streamflow and sea level data). High-latitude coasts typically experience strong seasonality in sea level extremes (e.g., Jin et al., 2023), while their timing depends on regional climatic and oceanographic conditions. In north-western Europe, for example, the highest mean and maximum sea levels are measured in the winter, and lowest in the spring, reflecting the patterns in the polar front westerlies (Johansson et al., 2001; Fernández-Montblanc et al., 2020). In the Arctic, the seasonality reflects thermal expansion of sea water, freshwater input, atmospheric circulation and sea ice formation, with sea level being highest after the thermal peak in the early autumn and lowest in the spring (Pavlov, 2001; Baumann et al., 2018; Jin et al., 2023). The variability of sea-level has changed in the high latitudes, with maxima increasing most markedly (Johansson et al., 2001; Omstedt et al., 2004; Barbosa, 2008). Globally, storminess is also expected to increase, driving more frequent and stronger storm surges on the coasts (Wahl et al., 2015). Streamflow in the high latitudes is to a large extent influenced by temperature and spring snow melt, creating distinct seasonal patterns in streamflow with high spring flood peaks that are typically an order of magnitude higher than peaks during the rest of the year (e.g., Bring et al., 2016). Due to climate change, the high-latitude winter season is shortening (Bring et al., 2016; Lintunen et al., 2024), and this may notably impact the co-variability of sea level and streamflow patterns. Increased storminess drives heavier rainfall, producing higher and more frequent streamflow peaks during open water conditions.

Few previous studies examine compound flooding in the high latitudes. Global (Couasnon et al., 2020 using the annual maxima approach) and continental-scale (Heinrich et al., 2023 using the peaks over threshold approach) analyses using simulated data indicate that the compound flood potential generally decreases with latitude, while distinct regional-scale patterns emerge. For example, the studies suggest strongest co-variance patterns and more frequent compound events along west-facing coasts (Couasnon et al., 2020; Heinrich et al., 2023). The study by Bevacqua et al. (2019) estimates short return periods in certain coasts of Iceland and Norway, and no clear patterns in the Baltic Sea. The same study predicts a significant increase in compound flood potential both in the northern and southern coasts of Finland, but not in the Bothnian Sea coast, and identifies the Baltic Sea as one of the European hotspots of increasing compound flood potential (Bevacqua et al., 2019). In contrast, the European study by Heinrich et al. (2023) argues that the number of compound flood days will decrease in the Bothnian Sea and Bothnian Bay coasts of Finland due to decreasing sea levels. However, their finding is based on stationary flood thresholds and non-detrended sea level simulation and thus reflects the impact of post-glacial rebound in this area. Thus, they are not directly examining changes in the compound flooding processes in the land uplift coasts.

The high-latitude coasts present a challenge for examining compound flooding due to strong hydrological seasonality and regionally varying relative mean sea level trends. The absolute post-glacial land uplift rates range from −1 mm per year in the southern Baltic Sea to + 10 mm per year in the north (Ekman and Mäkinen, 1996; Lidberg et al., 2007) and from −2 to + 10 mm per year along North American coasts (van der Wahl et al., 2009). Thus, in notable parts of the high-latitude coast land uplift is faster than the current sea level rise, resulting in relative sea level decline. This means also a declining base level for flood scenarios.

Compound flood events have been examined using multivariate statistical analysis of observations (e.g., Couasnon et al., 2018; Ganguli et al., 2020; Fang et al., 2021) and simulated data (e.g., Couasnon et al., 2020; Bevacqua et al., 2019). Extreme value theory and, for example, the copula theory have been applied to characterize bivariate joint distribution of high sea level and streamflow (Ward et al., 2018; Bevacqua et al., 2019). Currently, there is no common definition of a compound event (Couasnon et al., 2020), but several statistical methods have been suggested to identify them (e.g., Hao et al., 2018; Tilloy et al., 2019). In cold and high-latitude environments, annual maxima of discharge often occur during spring snow melt season, but storm surges rarely occur during this period. The widely used annual maxima approach for identifying flood events often catches spring snowmelt events, and may not capture high discharge events during other hydrological seasons (Wahl et al., 2015; Bevacqua et al., 2017; Zscheischler et al., 2018; Heinrich et al., 2023). We expect the peaks over threshold approach (POT; applied by, e.g., Fang et al., 2021; Heinrich et al., 2023; Kupfer et al., 2025) to be more appropriate for high-latitude coasts with distinct seasonality, as the threshold can be adjusted to capture high discharge events other than the spring snowmelt flood. To our knowledge, it has not been applied before to examine compound flood events in areas with geographically varying sea level trends, although Baldan et al. (2022) have highlighted the need for non-stationary analysis of sea level extremes.

This study aims to enhance understanding of compound coastal flood potential and its changes along the high-latitude coasts of the Baltic Sea. We concentrate on oceanographic-fluvial compound flooding and, due to the scarcity of direct water level measurements in estuaries, examine flood potential based on paired coastal sea level and river discharge measurements. Moreover, we explicitly separate relative sea level trends from short-term fluctuations, which enables a more direct examination of compound flooding caused by hydro-climatological processes. We address the main aim by answering the following research questions: 1. How does the compound flood potential vary spatially on the Finnish coast along the latitudinal gradient and the axis from the Baltic Proper coast toward the Baltic Sea gulfs? 2. What is the seasonality of compound flooding, and how it varies spatially? 3. How is compound flood potential changing at the decadal time-scale?

2. Material and methods

We investigated compound flood potential by analysing the co-variation of sea level and river discharge at 11 sites along the coast of Finland. We identified potential compound flood events – co-occurrences of high sea level and high streamflow – by examining how often they co-occurred during 1971–2024, and estimated their joint exceedance probability and return periods. We also examined the seasonality of the number of potential compound floods, and the temporal changes in the number of events.

All data management and analyses were conducted with the base functions of R software (4.4.1; R Core Team, 2024) and *dplyr* package (1.1.4; Wickham et al., 2023) unless otherwise stated.

2.1. Study area

The Finnish coast spans from approximately 60 °N to 66 °N (Fig. 1). The Archipelago Sea coast in southwestern Finland is closest to the Baltic Proper, the main basin of the Baltic Sea. From here, the Finnish coast extends northward and eastward towards the Bothnian Bay and Gulf of Finland, respectively. Due to the track of the main south-westerly weather systems approaching Finland from the Atlantic, there is a gradient from more maritime climate with mild winters in south-west to more continental one with distinct seasons in north-east. Historical relative land uplift rates (from the beginning of observations to 2018) vary greatly along the Finnish coast, from 0.9 mm per year in the south-east to 7.0 mm per year in the southern Bothnian Bay coast (Pellikka et al., 2023). In the future, rising global sea level will cause relative sea level rise in the eastern Gulf of Finland in the 21st century in all emission scenarios, while post-glacial uplift will likely continue to compensate it on the west coast of Finland from Rauma to Kemi (Pellikka et al., 2023).

The Baltic Sea has negligible tidal activity, but the sea level varies due to water exchange between the Baltic Sea and Atlantic, air pressure variation, winds and inflow from the catchment (Johansson et al., 2001; Barbosa, 2008; Pellikka et al., 2023). Sea level

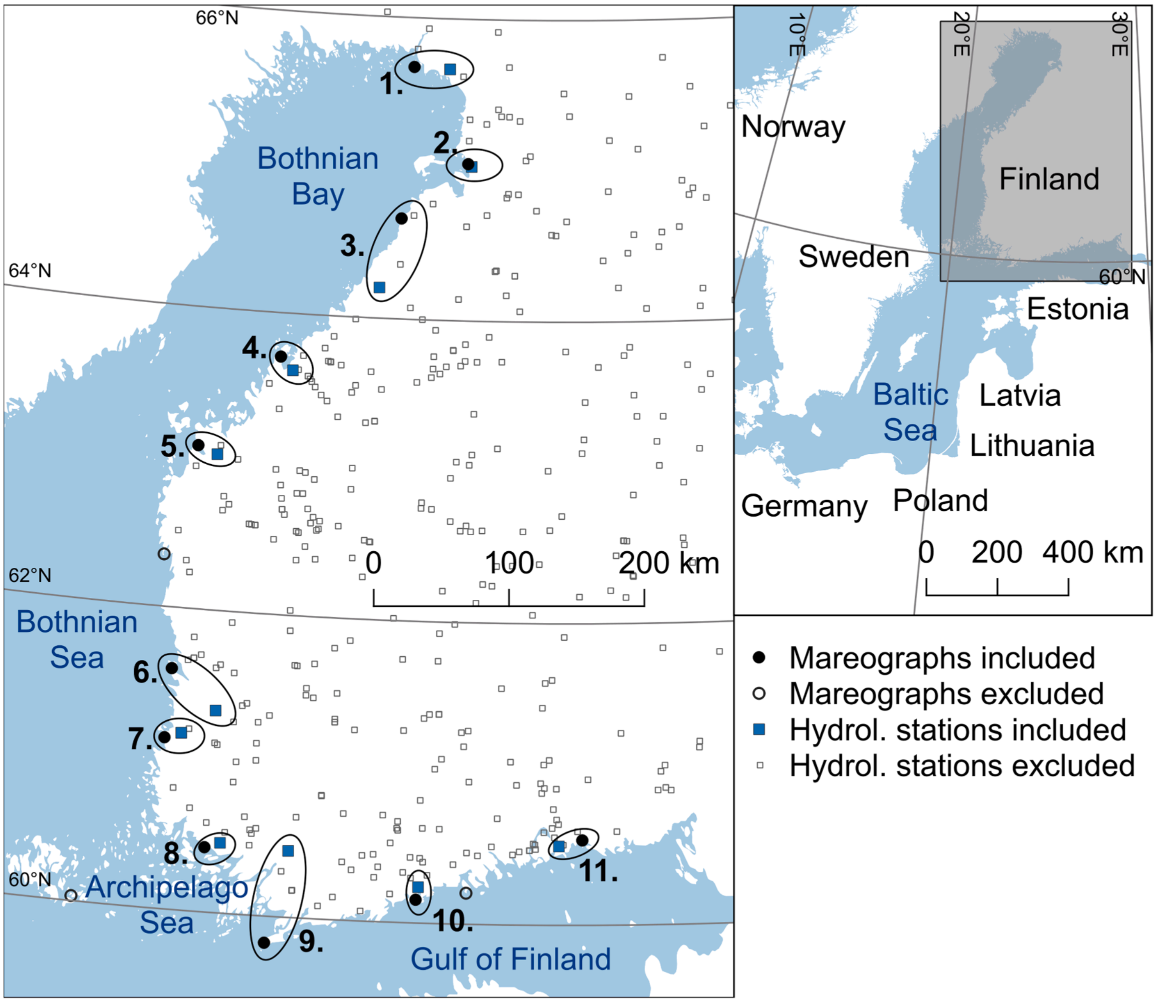

Fig. 1. Study area and sites 1.–11., consisting of 11 pairs of mareographs and hydrological stations (Table 1). Data: Station coordinates by Finnish Meteorological Institute and Finnish Environment Institute.

variation along the Finnish coast is smallest in the Archipelago Sea (southwest Finland), and increases both eastward and northward towards the Baltic Sea gulfs. Highest sea level variation of more than three meters occurs at the northernmost tip of the Bothnian Bay (Johansson et al., 2001; Wolski and Wiśniewski, 2020). Late autumn and winter are the stormiest seasons of the year, causing storm surges at the coast: highest sea level maxima therefore occur during these storms (Bierstedt et al., 2015; Fig. 2). Spring and summer are usually calm with very few storm surges. At longer time scales of weeks and months, sea level is related to the water exchange through the Danish straits (and NAO) and at short time scales with atmospheric low pressure systems (e.g., Barbosa, 2008; Zakharchuk et al., 2022). The most distinct change observed during the past decades is an increase in the sea level maxima in Finland and the Baltic Sea in general (Johansson et al., 2001; Barbosa, 2008).

Streamflow in the Finnish rivers draining into the Baltic Sea is strongly linked with the hydrological seasons. In the north, catchments and rivers freeze during winter months, and annual streamflow maxima occur in the spring when the snow melts (Fig. 2; Lintunen et al., 2024). In the winter, sub-zero temperatures and precipitation as snow keep river discharges at minimum. The duration of river ice cover is short in southern Finland, but up to five months in the northernmost Baltic Sea coast. During autumn and winter storms, heavy rainfall may cause rivers to flood if temperatures are above 0 °C. In spring, most of the Finnish rivers experience snow melt flooding. The spring floods begin in March in southern Finland and end in May in the north. In the south, high streamflow events occur during spring months, but also during autumn and winter storms before the catchments freeze (Fig. 2; Lintunen et al., 2024). However, streamflow patterns are changing with the climate: high-flow events are more evenly spread throughout the year, and streamflow of late autumn, winter, and early spring are increasing (Lintunen et al., 2024). While some of the major rivers in Finland are free-flowing, many of them are regulated, which may flatten streamflow peaks and impact lag times between rainfall and streamflow peaks.

2.2. Study sites

We examined 11 sites along the coast of Finland, using pairs of mareograph and hydrological station records (Table 1). All of the sites were located in the mainland coast of Finland (Fig. 1). Three of the Finnish mareographs were not examined in the study. Namely, the Föglö mareograph was excluded from the analyses, due to a lack of significant river estuaries in the Åland islands, Porvoo Emäsalo was excluded due to a short sea level time-series starting in 2014, and Kaskinen due to a lack of full discharge time-series in the surrounding rivers (all starting in the 1980s).

After the main analyses, we selected one of the identified potential compound flood events at site 6. Pori in February 2020. We extracted water level data for the entire hydrological year 2019–2020 to be able to compare the identified February event with other conditions.

2.3. Data

We matched sea level data from permanent mareographs along the Finnish coast (c.f., Finnish Meteorological Institute, 2025c) to river discharge data from permanent hydrological stations of major rivers close to the mareographs (c.f., Finnish Environment Institute, 2026; Table 2; Fig. 1). When multiple hydrological stations with long time-series were available, we chose the most downstream one. Sea level has been measured in the oldest Finnish mareograph in Hanko (south-west Finland) since 1887, but the open data used in this study are available from January 1st 1971.

In this study, we examined the 54-year period 1971–2024 for three reasons. First, it was considered long enough for examining general patterns in compound flood potential, and to draw some conclusions on recent trends reflecting climate change. Second, compared to longer periods, there were more mareograph and hydrological station pairs spanning this study period, allowing more geographical coverage in our analyses. Third, using open data only improved the reproducibility of our study.

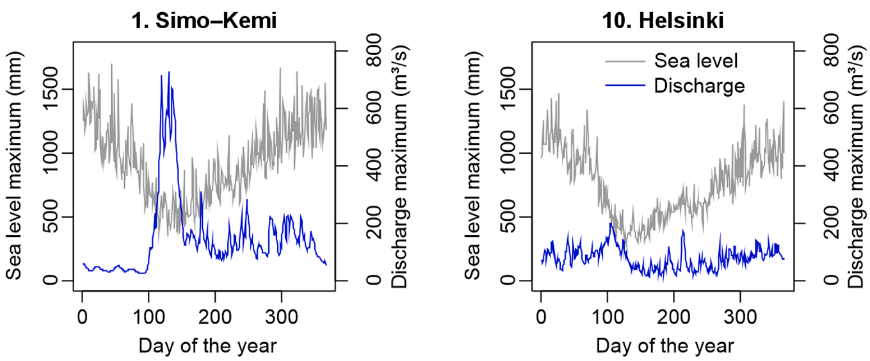

Fig. 2. Seasonality in sea level and river discharge maxima at sites 1. Simo–Kemi (66° N) and 10. Helsinki (60° N; Fig. 1; Table 1) in 1971–2024. The charts show daily sea level maxima by day of the year in Kemi, northernmost Finnish coast, and Helsinki in southern Finland. The daily discharge maxima are shown for the lower Simojoki river near Kemi, and for the lower Vantaanjoki river in Helsinki. Data: FMI Open Data WFS service by the Finnish Meteorological Institute (2025a), b) and SYKE Hydrology API by the Finnish Environment Institute (2025).

Table 1
Datasets used in the analysis. The year of the first water level observation in the Kokemäenjoki river varied between 1974 and 2022. FMI = Finnish Meteorological Institute, SYKE = Finnish Environment Institute.

Variable	Orig. interval	Dataset (Variable name)	Provider	Metadata	Years
Sea level (N2000, mm)	10 min	FMI Open Data WFS service (WLEVN2K_PT1S_INSTANT)	FMI	Finnish Meteorological Institute (2025a), (2025b)	1971–2024
River discharge (m^3/s)	Daily mean	SYKE Hydrology API (Virtaama)	SYKE	Finnish Environment Institute (2025)	1971–2024
Kokemäenjoki river water level (cm, converted to mm)	Daily mean	SYKE Hydrology API (Vedenkorkeus)	SYKE	Finnish Environment Institute (2025)	1974–2024

Table 2
The 11 sites in the coast of Finland (Fig. 1) and availability of daily sea level and discharge data during the 54-year period 1.1.1971–31.12.2024. The table also lists station numbers and names, the name of the river and the approximate straight-line distance between the mareograph and the hydrological station.

Site	Hydrol. station Mareograph	River Distance (km)	First obs.	N obs.	Obs. coverage (%)
1. Simo–Kemi	1349 Simo	Simojoki	1.1.1971	19724	100
	100539 Kemi Ajos	26.5	2.1.1971	19280	97.7
2. Oulu	1314 Merikoski	Oulujoki	1.1.1971	19724	100
	134248 Oulu Toppila	3.3	2.1.1971	19689	99.8
3. Kalajoki–	1253 Niskakoski	Kalajoki	1.1.1971	19722	> 99.9
Raahe	100540 Raahe Lapaluoto	53.8	1.1.1971	19686	99.8
4. Pietarsaari	1229 Herrfors	Esse å	1.1.1971	19609	99.4
	134250 Pietarsaari Leppäluoto	13.5	1.1.1971	19720	> 99.9
5. Vaasa	1204 Karkkimala	Laihianjoki	1.1.1972	19357	98.1
	134223 Vaasa Vaskiluoto	15.5	1.1.1971	19724	100
6. Pori	1188 Harjavalta	Kokemäenjoki	1.1.1971	19722	> 99.9
	134266 Pori Mäntyluoto Kallo	45.0	1.1.1971	19343	98.1
7. Rauma	1122 Ylinenkoski	Lapinjoki	1.1.1971	19662	99.7
	134224 Rauma Petäjäs	12.9	1.1.1971	19717	> 99.9
8. Turku	1117 Halinen	Aurajoki	1.1.1971	19666	99.7
	134225 Turku Ruissalo Saaronniemi	12.0	1.1.1971	19718	> 99.9
9. Salo–Hanko	1111 Kaukolankoski	Uskelanjoki	1.1.1971	19521	99
	134253 Hanko Pikku Kolalahti	70.5	1.1.1971	19724	100
10. Helsinki	1097 Oulunkylä	Vantaanjoki	1.1.1971	19724	100
	132310 Helsinki Kaivopuisto	9.5	1.1.1971	19723	> 99.9
11. Kotka–	1065 Koivukoski	Kymijoki	1.1.1971	19722	> 99.9
Hamina	134254 Hamina Pitäjänsaari	17.9	1.1.1971	19722	> 99.9

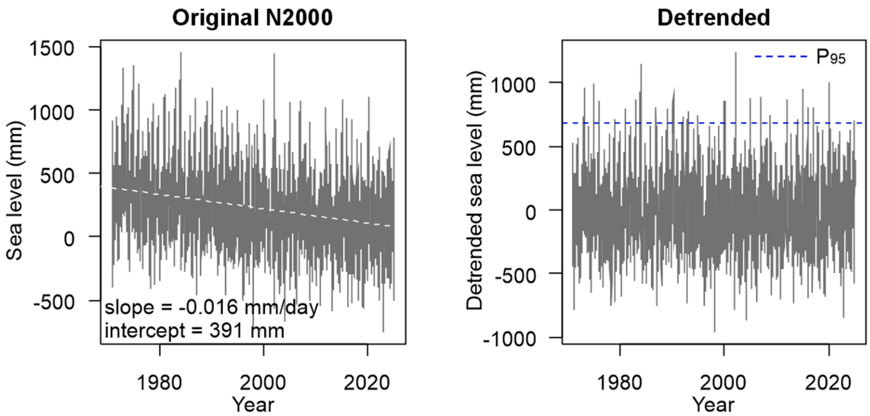

Fig. 3. Detrending sea level time-series: an example from site 5. Vaasa (63° N; Fig. 1), in the Bothnian Sea coast of Finland with the highest relative land uplift rate in Finland. Percentile P_{95} of the detrended sea level time-series is also shown in the right. The left panel indicates the raw coefficients of the linear model (with daily time-series), the intercept in mm in January 1st 1970. Data: Sea level data for Vaasa Vaskiluoto from the FMI Open Data WFS service by the Finnish Meteorological Institute.

The sea level and discharge time-series were filtered to a common analysis period between 1971 and 2024, and missing values were omitted from the analyses. We then calculated the daily mean sea level from the original 10-minute interval data, to match the frequency with discharge observations.

After analysing the co-variation of sea level and river discharge, we compared the findings against water level observations (Finnish Environment Institute, 2026) in the lower Kokemäenjoki river in the Bothnian Sea coast (Table 2), where the water level station network has been notably densified in the first decades of the 21st century. We looked for coinciding water level data in all mainstream stations that were located downstream of the Harjavalta discharge station. Water level data were found from five stations (stations a.–e.; station ids 3744, 3278, 3321, 3692, 3693), providing a good coverage in the Kokemäenjoki estuary (appendix Figure A.1). To compare water levels along the course of the river and to allow comparison to sea level, we converted observations measured in a station-specific elevation system to the common N2000 vertical datum using level correction information for each station (attribute “VedenkTasoTieto”) reported by the Finnish Environment Institute (2025). Sea level and river water level observations were converted to the same units, millimetres relative to N2000.

2.4. Methods

The analyses aimed at identifying compound flood events from paired station records, examine their spatial, decadal and seasonal patterns, and to estimate the compound flood potential by examining the high-tail dependence structure of sea level and river discharge.

We used the local mean sea level, measured relative to the uplifting land, as the baseline for examining sea level peaks. To account for the mean sea level trend, the flood thresholds and flood peaks were determined from a detrended sea level time-series, after eliminating a linear trend between 1971 and 2024 (Fig. 3; c.f., Coles, 2001; Stephens et al., 2020; Luxford and Faulkner, 2020; Lyddon et al., 2023). Linear trend slopes for each site are reported in appendix Table A.1 and their spatial distribution – that reflects land uplift patterns in Finland – is shown in the appendix Figure A.2.

To facilitate identification of potential compound events that occur outside the spring snowmelt flood period, we repeated analyses using two variants of the datasets: a full year-round dataset including all observations, and a “seasonal” dataset excluding observations during the spring snowmelt season. To extract the seasonal dataset, we first calculated mean discharge curves for the hydrological year (hydrograph) from the full 1971–2024 time-series, and applied smoothing using the Locally Estimated Scatterplot Smoothing algorithm (R function *loess*; R Core Team, 2024). We then identified the snowmelt window separately for each site, as the time period with smoothed discharge values exceeding the 85th percentile and occurring between March 15th and June 31st (appendix Table A.1; appendix Figure A.3). We then excluded this period from the “seasonal” time-series. The spring snowmelt windows are listed for each site in the appendix Table A.1. Based on these criteria, no spring flood window was found for the Merikoski hydrological station in Oulujoki, and therefore no “seasonal” analysis was done for the site 2. Oulu.

The identification of potential compound floods was based on the application of the peaks over threshold approach (e.g., Fang et al., 2021; Heinrich et al., 2023; Kupfer et al., 2025). Flood peaks were identified for sea level and river discharge based on site-specific percentile thresholds. We performed a sensitivity analysis following Fang et al. (2021) to test how the choice of threshold (90–99%) impacted the number of identified high-tail pairs (sea level and discharge exceeding the threshold simultaneously) and the tail correlation of sea level and discharge. The analysis showed that the threshold influenced the strength of the correlation, but the correlation generally remained stable for thresholds 90–96% (appendix Figure A.4). Beyond this, the decreasing number of tail pairs made the correlation less stable. For example, for the northernmost site 1. Simo–Kemi, not a single tail pair was found with thresholds exceeding 95% (appendix Figure A.4). Based on the sensitivity analysis, we applied the 95th percentile threshold (hereafter P_{95}) for all sites to extract enough sea level and discharge peaks for examining co-variation, and not only the extreme values for each variable. Working with more than 100 peaks at most sites facilitated correlation analysis (c.f., Lyddon et al., 2023). Thus, percentile P_{95} threshold was calculated for discharge and for the detrended sea level time-series (Table 3).

We then identified dates when (1) sea level, (2) discharge, or (3) sea level and discharge simultaneously exceeded their respective

Table 3
Percentile P_{95} thresholds and the number of identified sea level and discharge events (multi-day high value events separated by three days or less) for analyses at the 11 sites (Fig. 1; Table 1). For sea level, the thresholds and events were identified from the detrended time-series. Discharge thresholds were calculated separately for the full datasets and for the “seasonal” dataset, excluding the station-specific spring snowmelt period. [1] No seasonal window was found for the Merikoski station, and therefore no seasonal analysis was performed at site 2. Oulu.

Mareograph (site number)	Thresh. (mm)	Events	Hydrol. station	Thresh. (m^3/s)	Events	Thresh. seasonal	Events seasonal
Kemi Ajos (1.)	548	451	Simo	143	92	73	110
Oulu Toppila (2.)	528	423	Merikoski[1]	459	192	-	-
Raahe Lapaluoto (3.)	502	403	Niskakoski	124	173	88	158
Pietarsaari Leppäluoto (4.)	462	339	Herrfors	31	101	29	82
Vaasa Vaskiluoto (5.)	423	257	Karkkimala	13	216	10	201
Pori Mäntyluoto Kallo (6.)	405	246	Harjavalta	497	122	478	97
Rauma Petäjäs (7.)	401	235	Ylinenkoski	14	114	12	110
Turku Ruissalo Saaronniemi (8.)	401	225	Halinen	31	288	26	281
Hanko Pikku Kolalahti (9.)	408	211	Kaukolankoski	22	339	18	309
Helsinki Kaivopuisto (10.)	451	272	Oulunkylä	62	193	50	184
Hamina Pitäjänsaari (11.)	510	354	Koivukoski	172	62	171	57

P_{95} thresholds, and clustered them to multi-day single-driver and compound events separated from each other by more than three days (Table 3). For example, high values on December 14th, December 15th and December 17th formed one four-day event. The clustering and the chosen lag time of three days followed the methodology of previous studies (e.g., Fang et al., 2021; Heinrich et al., 2023). We then counted how many potential compound events occurred in the full dataset and during the non-snowmelt seasons. We also calculated the mean and maximum duration of compound events in the full dataset.

We estimated the probabilities and return periods of compound events (joint P_{95} exceedances) at the event scale. We first modelled the exceedances of sea level (S) and discharge (Q) above their respective 90th percentile thresholds with Generalized Pareto Distributions (GPDs). This resulted in marginal distributions F_s and F_Q. The fitted GPD model allowed us to transform the maximum sea level and maximum discharge value of joint over P_{90} events into a uniform scale, u_S and u_Q, (between 0 and 1) for copula modelling. GPDs were fitted with the *evir* R package (version 1.7–4; Pfaff and McNeil, 2018).

Using the GPD-transformed joint event data (u_S and u_Q), we fit a bivariate Gumbel copula $C(u_S, u_Q)$ to model the statistical dependence between upper tail sea level and discharge with the *copula* R package (version 1.1–6; Hofert et al., 2024). This enabled us to capture how strongly the two variables tended to covary during high sea level and high discharge conditions, and was done separately for the full dataset and for the seasonal dataset. The goodness-of-fit of the Gumbel copula models were estimated with a parametric bootstrapping test that compared the empirical dependence structure to the fitted copula. The goodness-of-fit was also compared to those of alternative Clayton and Gauss copulas. The goodness-of-fit results (appendix Table A.2) supported the use of the Gumbel copula throughout most of the sites, but it didn't fit ($p < 0.05$) the high-tail observations of sites 10. Helsinki ("seasonal" dataset only) and 11. Kotka-Hamina well. Despite this, the Gumbel copula was retained for consistency among sites and because it generally outperformed the other two copula candidates (appendix Table A.2).

Copula-based joint exceedance probability for thresholds s and q was calculated as:

$$P(S > s, Q > q) = 1 - u_S - u_Q + C(u_S, u_Q) \tag{1}$$

where $u_S = F_S(s)$, $u_Q = F_Q(q)$

From the copula model, we calculated the conditional (given that sea level and discharge exceed P_{90}) joint exceedance probability for joint peak events over P_{95} as:

$$P(S > s, Q > q \mid S > u, Q > v) = 1 - u^*_s - u^*_Q + C(u^*_s, u^*_Q \tag{2}$$

where $u^*_S = F^*_S(s)$, $u^*_Q = F^*_Q(q)$ are conditional marginal distributions.

This probability was converted into an event-based (unconditional) exceedance probability of potential compound flood events following, for example, Couasnon et al. (2020) as:

$$P_{event}(S > s, Q > q) = P(S > s, Q > q \mid S > u, Q > v) * \lambda \tag{3}$$

where λ = the event rate, and which can be also expressed as a return period T as:

$$T = 1 / (\lambda * P(S > s, Q > q \mid S > u, Q > v)) \tag{4}$$

In addition to this main analysis, we quantified the overall statistical relationship of daily sea level and discharge observations by calculating Kendall's τ for the full and seasonal time-series. We also identified the annual maxima of sea level and discharge and quantified their covariance by calculating Spearman's ρ, and examined how many of them co-occurred or were separated by three days or less, indicating potential compound flooding around annual maxima.

To identify seasonality in compound flood potential, we examined the number the sea level, discharge and compound events occurring during calendar months and quarters of the year (Q1 January–March, Q2 April–June, Q3 July–September and Q4 October–January). We calculated the number of calendar months during which potential compound events were found and the proportion of compound events occurring during the autumn quarter (Q3 July–September). Finally, we calculated the number of compound flood events in five-year time-steps starting from 1971 to 1976 and examined the temporal patterns in event numbers.

3. Results

3.1. Spatial patterns in compound flood potential

The number of potential compound flood events over the P_{95} thresholds ranged from less than 10 to almost 90 during the 54 years (Table 4). It was highest in south-west Finland (sites 8.–10.) and decreased northwards (only 6 events at site 1. Simo–Kemi) and eastwards (Table 4; Fig. 4a). When the snowmelt season was excluded, the analysis identified a notably higher number of potential compound events at the northernmost sites (for example, 36 in 1. Simo–Kemi; Table 4; Fig. 4b).

The joint exceedance probabilities were highest in the south-west coast of Finland, in an area spanning from sites 8. Turku to 10. Helsinki, and decreased northward and eastward (Table 4; Fig. 4c–d). The spatial patterns were similar for the "full" and "seasonal" datasets (Table 4; Fig. 4c–d). The return periods for joint sea level and discharge events over P_{95} ranged from 351 days at site 7. Salo–Hanko in the Archipelago Sea coast to over 1600 days at the northernmost site 1. Simo–Kemi (Table 4). This corresponds to events occurring once a year in the Archipelago Sea coast and every four years in the north. When the snowmelt period was excluded from the analyses, the return period decreased by approximately 10 and 15% in the south and north, respectively (Table 4).

The mean duration of potential compound events was c. two days at most of the sites, but notably higher at the two Bothnian Sea

Table 4

Statistics for the identified compound events, their probabilities and return periods at the 11 sites (Fig. 1; Table 1) in Finland. The table also reports Kendall's τ for daily sea level (detrended) and discharge observations, Spearman's ρ for the 54 annual maxima and the number of co-occurring annual maxima. Compound events were defined as sea level and discharge peaks over P_{95} occurring within three days of each other, and their probabilities and return periods were calculated using copula modelling fitted to observations above P_{90}. The table reports values calculated from both the full dataset and a seasonal dataset excluding the spring snowmelt season (see appendix Table A.1). Values reflecting highest compound flood potential are highlighted with bold text. [1] No seasonal window was found for site 2. Oulu, and therefore no seasonal analysis was performed.

Site	1. Simo–Kemi	2. Oulu[1]	3. Kalajoki–Raahe	4. Pietarsaari	5. Vaasa	6. Pori	7. Rauma	8. Turku	9. Salo–Hanko	10. Helsinki	11. Kotka–Hamina
N compound	6	37	23	37	47	51	46	**88**	**87**	**61**	27
N comp. seasonal	36	-	39	44	65	56	58	**100**	**102**	**93**	27
Probability (%)	0.06	0.16	0.11	0.08	0.17	0.14	0.14	**0.26**	**0.29**	**0.20**	0.12
Probability seasonal (%)	0.07	-	0.13	0.10	0.20	0.15	0.17	**0.28**	**0.32**	**0.23**	0.13
Return period (days)	1620	626	937	1221	595	732	703	**383**	**351**	**492**	826
Return per. seasonal (days)	1364	-	781	1019	504	667	598	**356**	**317**	**436**	768
Mean duration (days)	1.7	2.6	2.1	2.5	2.4	**5.0**	**4.3**	2.0	2.0	2.6	3.3
Max duration (days)	3	12	8	8	9	**41**	**14**	8	13	**16**	10
τ daily obs. (n ≈ 19 500)	0.06	0.07	0.10	0.10	0.15	0.14	0.17	**0.21**	**0.23**	**0.20**	0.05
τ daily obs. seasonal	0.18	-	0.20	0.16	0.25	0.19	0.25	**0.28**	**0.30**	**0.29**	0.05
ρ annual max. (n = 54)	0.19	-0.02	-0.19	-0.22	-0.13	**0.22**	0.15	**0.22**	0.13	0.05	0.12
N annual max compound	0	2	1	1	1	**5**	**7**	4	**5**	4	3

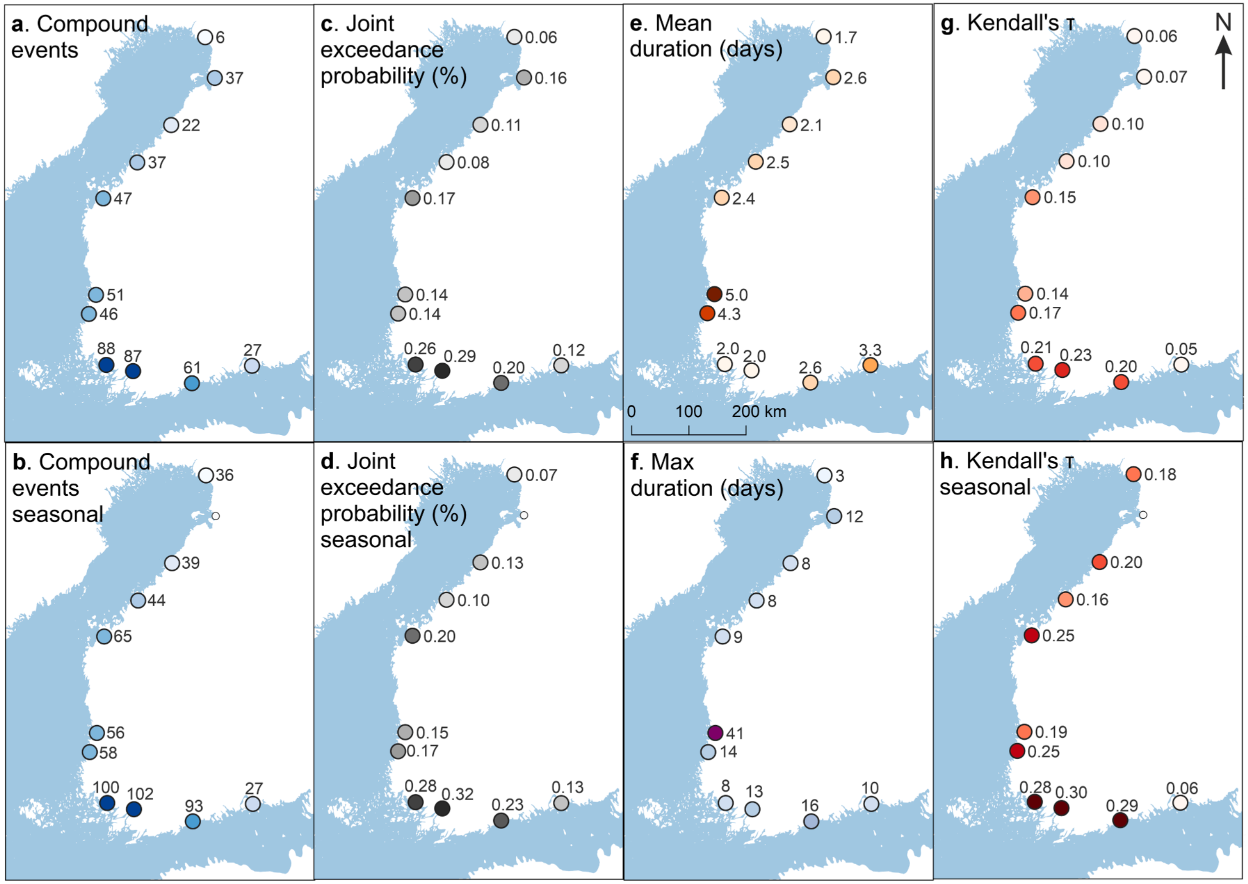

Fig. 4. Spatial distribution of (**a–b**) potential compound events over P_{95}, (**c–d**) joint exceedance probability, (**e**) mean and (**f**) maximum duration of the events, and (**g–h**) Kendall's rank correlation τ between daily sea level (detrended) and discharge observations at the 11 sites (Table 1) in 1971–2024. Compound events were defined as sea level and discharge peaks occurring within three days of each other, and their probabilities were calculated using copula modelling fitted to observations above P_{90}. The figure reports values calculated from both the full dataset (a, c, e, f, g) and the seasonal dataset (b, d, h) excluding the spring snowmelt season (see appendix Table A.1).

Journal of Hydrology: Regional Studies 66 (2026) 103551

sites, namely 6. Pori and 7. Rauma (5.0 and 4.3 days, respectively; Table 4; Fig. 4e). The maximum event duration was c. ten days, with a large range from three days at the northernmost site 1. Simo–Kemi to 41 days in 6. Pori (Table 4; Fig. 4f).

The overall correlation between sea level and discharge in Finland in 1971–2024 was relatively low, with Kendall's τ spanning from 0.05 to 0.23 (Table 4; see also appendix Figure A.5 for the daily distributions). The positive association was strongest in the south-western coast of Finland, namely at the sites 8. Turku, 9. Salo–Hanko and 10. Helsinki, and decreased from Hanko to almost zero both northward towards the Bothnian Bay and eastward in the Gulf of Finland (Table 4; Fig. 4g). When the spring snowmelt period was excluded from the analyses, the correlation strengthened notably at the northernmost sites, as at the site 1. Simo–Kemi from 0.06 to 0.18 and at the site 3. Kalajoki–Raahe from 0.10 to 0.20 (Table 4; Fig. 4h). The increase in Kendall's τ was less substantial at the southern sites (Table 4).

The correlation of annual maxima in sea level and discharge was generally too low for making conclusions based on the 54 observations. It varied from negative in the north (except site 1. Simo–Kemi with positive Spearman's ρ) to positive in the south (Table 4). During the 54 examined years there were only 0–2 compound annual maxima in the north, and 3–7 in the south (Table 4).

3.2. Seasonality of compound events

The mean monthly pattern of potential compound flood events in Finland showed a distinct peak in November and December, and the compound flood season generally lasted from October to March (Fig. 5). During the peak month of December, there were on average 13 potential compound flood events during the examined 54 years. During the other half of the year from April to September the number of compound flood events was very low (0–1 event per month, on average; Fig. 5; quarterly distribution in appendix Figure A.6).

At the northernmost sites, particularly 1. Simo–Kemi and 3. Kalajoki–Raahe, the seasonal sea level and discharge patterns differed from each other so much that there was in practice no potential for compound events (Fig. 5). Namely, sea level peaks occurred between September and March and discharge peaks during April and May. The few potential compound flood events occurred in the north in November and December. At the central and southern sites, and interestingly also at site 2. Oulu, the seasonal discharge pattern was more even and compound events occurred also during the winter season, from January to March (Fig. 5).

Reflecting this seasonal pattern, the number of calendar months during which potential compound flood events were observed was smaller at the northern sites 1. and 3. (3–5 months) than at the rest of the sites (7–9 months; Fig. 6). In the north, almost all compound flood events were observed during late autumn months October, November and December, while in the central and southern Finland the proportion was less than two thirds (Fig. 6). Two sites deviated from this pattern: the potential compound events were more evenly distributed between calendar months than expected at sites 2. Oulu and 11. Kotka–Hamina, that represented streamflow patterns in the strongly regulated Oulujoki and Kymijoki, respectively.

3.3. Temporal trends in compound events

The number of observed potential compound flood events was relatively stable in 1971–2024 at the national scale when examined across five-year time-steps (Fig. 7). While no notable trends were present at the central and southern sites 5.–11., a slight increase in the event frequency could be detected at the northern sites 1.–4. (Fig. 7). Generally, there were less events during 1991–2005 than during the rest of the time-series, both nationally and in most sites (Fig. 7).

3.4. Case study: potential compound flood in Pori

One of the highest potential compound flood events of the 2020 s in Pori (61.5° N; Fig. 1) took place during 11.–28.2.2020. During the 18-day event, the maximum observed sea level in the Pori mareograph was + 940 mm (relative to the N2000 vertical datum) and the discharge in the Harjavalta station reached 657 m^3 /s (Fig. 8). To examine this event in a larger context, we inspected water level variation and different types of peaks during the entire hydrological year 2019–2020. Some of the sea level peaks were extreme, as the lowest national warning level for Pori, + 850 mm ("yellow" risk level; Finnish Meteorological Institute, 2026), was exceeded. The time-series revealed that both sea level and discharge stayed high the entire winter season, and the examined February event was actually surrounded by eight other events that our analysis identified as potential compound flood events occurring between December 2019 and March 2020 (Fig. 8). The exceptional winter was followed by an exceptional spring, with no notable spring flood.

Our examination concentrated on four distinct water level events. Event 1 in September 2019 was a (relatively) high sea level event with steady low discharge, event 2 in November 2019 a (relatively) high discharge event with low sea level, event 3 in December 2019 an extreme high discharge event with moderately high sea level, and event 4 in February 2020 a potential compound event with extremely high sea level and extremely high discharge (Fig. 8).

During the high sea level event 1, water surface slope remained very low between stations a. and e. corresponding to the lowermost 16 kilometres of the river (height difference of approximately 100 mm between stations; Fig. 8). The water level in the river was less than 100 mm higher than in the sea, causing the rising sea level to raise and falling sea level to lower the water surface in all stations. Thus, the impact of the sea was visible more than 15 kilometres upstream in low-discharge conditions (Fig. 8). During the high discharge event 2, the slope of the river surface increased notably (Fig. 8). Despite discharge being about six times as high as during event 1, the low sea level allowed the river water level to drop at the three lowermost stations c.–e. By contrast, water level upstream, at stations a. and b., was higher than during event 1 (Fig. 8).

During event 3, the doubled discharge compared to event 2 created a very high river surface slope and a surface height difference of

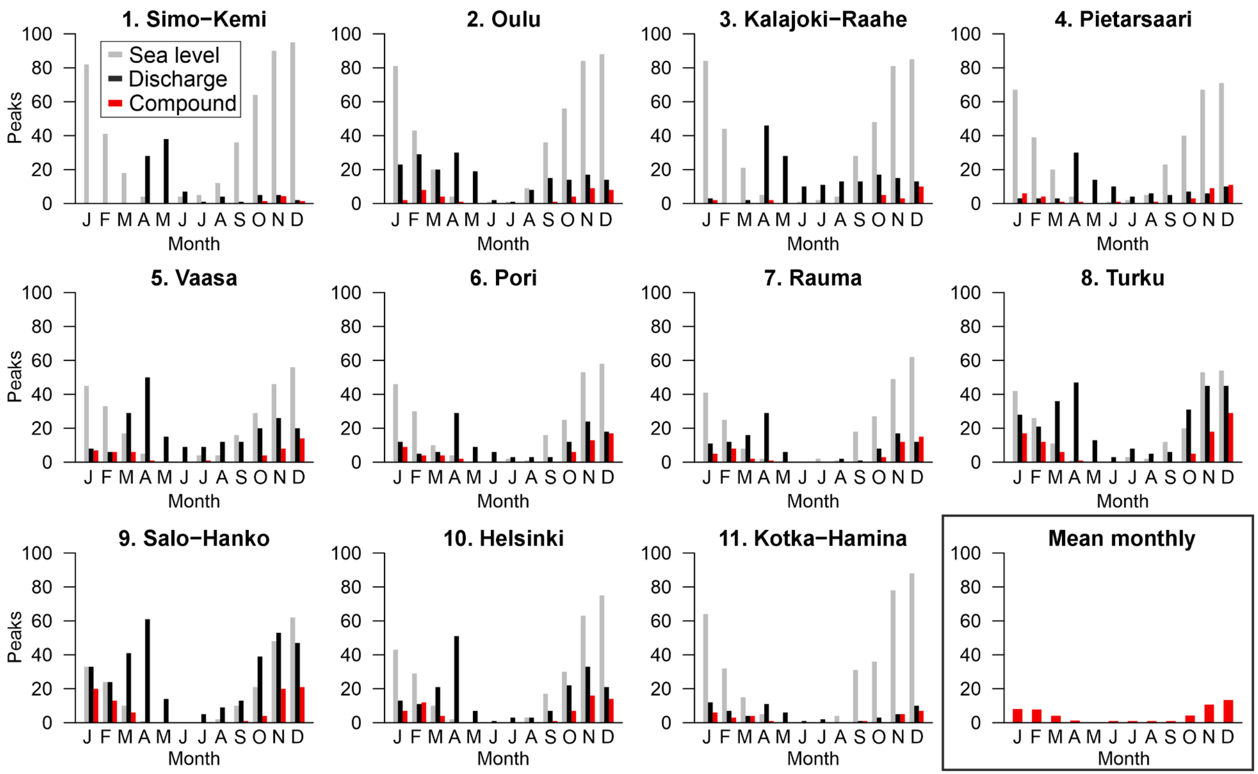

Fig. 5. Monthly distribution of peaks over P_{95} of sea level and discharge, and potential compound events at the 11 sites (Fig. 1; Table 1) and the corresponding monthly means in Finland during 1971–2024.

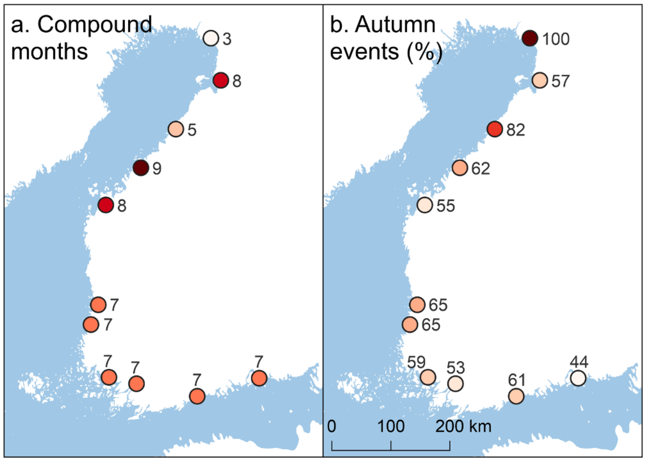

Fig. 6. Spatial distribution of **(a)** the number of calendar months with potential compound flood events and **(b)** the proportion of compound events taking place during late autumn months October, November and December, at the 11 sites (Table 1) in Finland during 1971–2024.

approximately 1.25 m between stations a. and e. (Fig. 8). At all stations, the shape of the water level curve mimicked that of discharge rather than sea level. Even though the sea level was also higher than on average, river water level at the lowermost station remained 500 mm higher than sea level during the event (Fig. 8).

During the potential compound event 4, water level in all of the five stations was higher than during event 3, despite comparable discharge (Fig. 8). The difference between water level peak heights between events 3 and 4 increased downstream, being approximately 200 mm at station a. and almost 500 mm at station e., and was also seen in a lower surface slope during event 4. This difference reflected the notably higher sea level during event 4 (Fig. 8). At station e., the local flood warning level (1140 mm; Waterinfo.fi, 2025) was exceeded during event 4 and stayed above it for several days. Even though discharge was as high during event 3 in December, the water surface did not rise above the flood warning level.

4. Discussion

Our study generates new insights into compound flooding, its seasonality and long-term trends at high latitudes through a case study in the Baltic Sea coast of Finland. We provide the first description of compound flood potential along the Baltic Sea coast of Finland that is based on paired sea level and streamflow observations spanning more than 50 years and taking fully into account the geographically varying seasonality and sea level trends. The examined coastline covers a wide latitudinal range (60°–66° N), allowing explicit examination of the impact of critical shift in winter climate on compound flood potential.

Our findings are largely consistent with previous studies using simulated data in that the compound flood potential is highest in the south-west Finland close to the Baltic Proper and decreases northward and eastward towards the Baltic Sea gulfs (Couasnon et al., 2020; Heinrich et al., 2023). Based on historical data, the compound flood potential is lowest in the northernmost coast of Finland (c.f., Bevacqua et al., 2019, Couasnon et al., 2020). Our results indicate clearer spatial patterns with smaller differences between neighbouring sites than the studies of Couasnon et al. (2020) and Bevacqua et al. (2019). We show that three sites of the south-west coast between Turku and Helsinki have the highest co-variability of sea level and streamflow and the highest number of potential compound flood events, identified as co-occurring peaks over threshold. Couasnon et al. (2020) indicate that the co-variability of annual maxima is similarly highest in two south-west sites, but do not reveal that outside the annual peak values, there is high co-variability in a larger geographical area, including the coast of Helsinki in the western Gulf of Finland.

The previous studies on the Finland coast do not examine compound flood event duration. Our results indicate that the event duration has less clear spatial pattern and more site-specific variation than event frequency. While the mean duration in most of the sites is two days (measured with daily observations), it is twice this long in two sites at the Bothnian Sea coast that are not among the highest-frequency sites. This longer event duration may have consequences on the local ecosystems and human communities. The historical maximum duration of potential compound flood events ranges from three days (northernmost site) to 41 days (site near the city of Pori in the Bothnian Sea coast) in Finland, being highest in the two Bothnian Sea sites and in Helsinki.

The results, showing that most of the compound events occur in the Baltic Sea coast of Finland between October and March, and particularly in November–December, support the general finding from northern Europe that the role of the autumn and winter storms

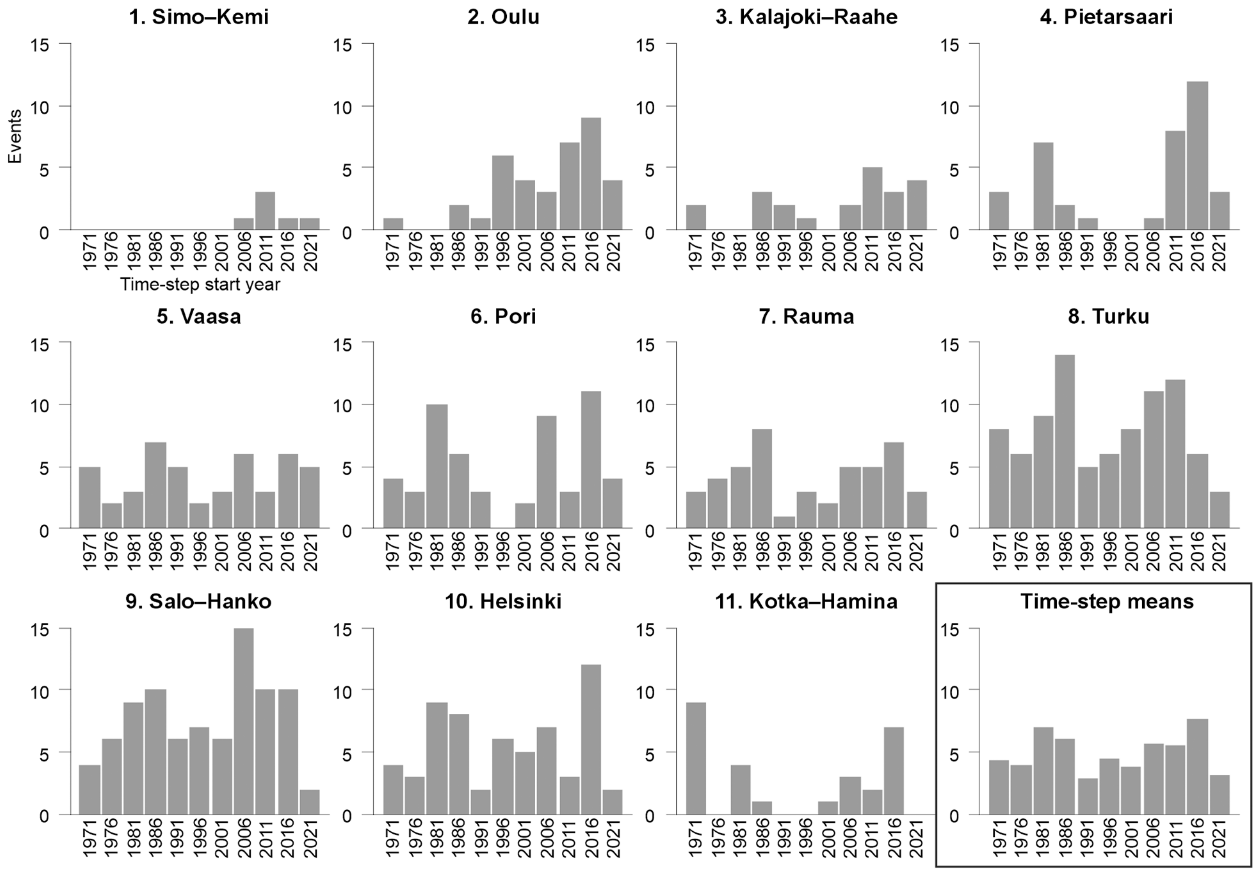

Fig. 7. Distribution of compound events at the 11 sites (Fig. 1; Table 1) and the corresponding means in Finland between five-year time-steps between 1971 and 2024. Note that the last time-step consists only of four years.

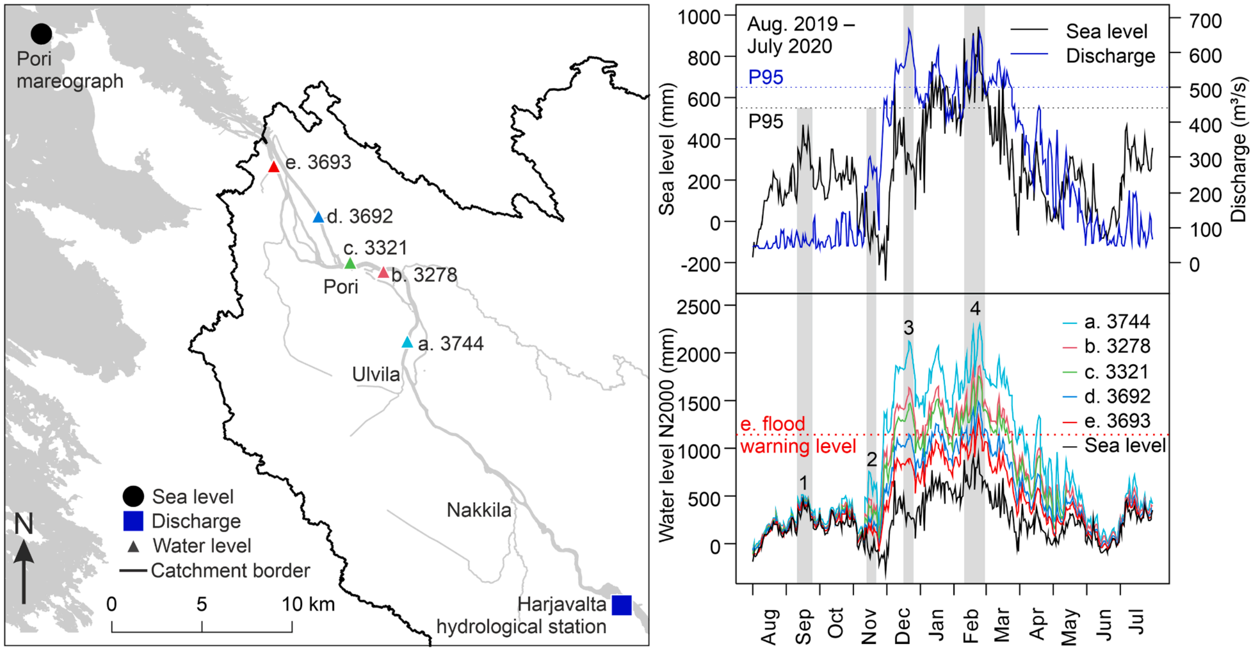

Fig. 8. Variation in sea level, upstream river discharge and downstream water level at five stations (a.–e.) in the lower Kokemäenjoki catchment at site 6. Pori (61.5° N; Fig. 1) during the hydrological year 2019–2020. Events 1–4, including the potential compound event 4 in 11.–28.2.2020, are highlighted. Percentile P_{95} of detrended sea level was transformed back to the original scale of sea level observations, i.e., N2000 vertical datum (554 mm). Local flood warning level 1140 mm for station e. is also shown (Waterinfo.fi, 2025).

in determining the compound flood season is very important (e.g., Heinrich et al., 2023). The proportion of the autumn events is very high in the north, where temperatures generally remain below zero during the winter months and precipitation is stored in the snowpack, while the number of winter events increases to the south. This suggests that snow accumulation and snow melt dictates the likelihood of co-occurring peaks in sea level and streamflow in the high latitudes. In areas where the catchment is frozen and precipitation accumulates in solid state during the winter months and there is a distinct snowmelt flooding in the spring, the highest peaks unlikely co-occur. In areas where the catchments receive more of the winter precipitation as rain and the rivers flow open longer, there are more opportunities for simultaneous storm surges raising the sea level and streamflow peaks raising water level in the rivers. This finding indicates that the compound flood potential may change in the near future particularly in the northern Baltic Sea area, as a response to changes in the winter season. A similar pattern is expected along other high-latitude coasts experiencing rapid cryospheric change.

Our results suggest that there are notable geographical differences in how compound flood potential is changing over time. Namely, there are currently no clear trends at the national scale in Finland, but differences between southern and northern Finland are evident. The number of potential compound flood events has been increasing in northern Finland, particularly in the Gulf of Bothnia. Since we separated the compound flooding process from the impact of long-term sea level trends, we were able to demonstrate this trend for northern Finland. In contrast, Heinrich et al. (2023) conclude that compound flood potential is seemingly decreasing in the areas with land uplift, namely the Gulf of Bothnia, as they did not remove the sea level trend from the observations. Naturally, post-glacial land uplift along the Gulf of Bothnia coast will reduce the adverse impacts of compound flooding on infrastructure whose elevation relative to the mean sea level is increasing.

There are notable differences in the temporal trends of compound flood potential between sites in southern Finland, with neighbouring sites having opposite trends. The compound flood potential and its changes over time may reflect local catchment characteristics (e.g., catchment and channel geometry and orientation) and processes, including changes in land cover and land use, or regulation of the rivers. The data also indicate decadal differences in compound flood potential, with less events occurring in the 1990s compared to 1980s and early 2000s. These decadal differences superimposed on long-term trends may reflect decadal variation in sea level of the Baltic Sea (e.g., Karabil et al., 2017).

Our case study in the Kokemäenjoki river in the west coast of Finland (one of the two Bothnian Sea sites) indicates that the peaks over threshold method coupled with aggregating observations into multi-day events is able to identify true compound flood events among single-driver floods, and separate longer events (including days just below the thresholds) from short isolated peaks. We also show for this site that back-transforming the identified flood thresholds and compound event flood heights from the de-trended sea level data into the national datum is straightforward. The case study clearly demonstrates how equal discharge peaks lead into different downstream flood heights depending on sea level. During a compound flood estuarine water level is higher than during a single-driver river flood over a long section of the river (more than 16 kilometres in the Kokemäenjoki river). The impact of sea level increases downstream and the surface slope of the river is lower than it would be in low sea level conditions. We demonstrate how the compound event leads to conditions where the local flood warning level is exceeded in the city of Pori, while it is not exceeded during comparable single-driver conditions. This finding indicates a need for more detailed coupling of the paired station records and estuarine water level observations in estuary types with different hydrodynamic conditions, which in turn calls for direct water level measurements in the estuaries.

Estuary types that vary in geometry, catchment features, land cover and land use have distinctly different compound flood potential. Our study sites represent a wide range of estuary types. For example, streamflow of the Oulujoki in site 2. is heavily influenced by a large lake (Oulujärvi) and artificial regulation while other northernmost rivers included in our study have lower lake percentage and are unregulated. Examining the local processes superimposed on the regional ones is, however, beyond the scope of this study. Moreover, our study setting varies between sites, preventing direct comparisons. Most importantly, the straight-line distances, along-stream distances and elevation difference of the paired mareograph and discharge stations vary between sites, which is bound to impact the level of co-variability seen in the sea level and discharge records, and potential lag times. The impact of the paired station distance on identified compound flood potential would deserve a dedicated study.

Studies on compound flooding are mainly based on paired observations of sea level and discharge, like in our case, or simulations, because of missing water level observations in the estuaries. Based on these comparisons of best available data, it is not possible to directly examine water level in estuaries. Our case study is one of the few examples coupling paired observations and direct water level measurements in the downstream section of a river (see, however, McKeon and Piecuch, 2025). It clearly shows how important it would be to measure water level in different types of estuaries for developing our understanding of compound flooding and to estimate consequent flood risk for the coastal cities. Such data would in the future open up new possibilities for examining the development of the compound flood events at the estuary scale. In other words, water level measurements in different parts of the estuary could allow analysis of how the timing and amplitude of the flood varies at the downstream–upstream axis and the cross-channel axis, or between open and more sheltered parts of the estuary.

In addition to the general spatial patterns of compound flood potential in Finland, our study identified outliers that break the overall pattern that may reflect local environmental conditions or differences in the study setting. For example, the analyses indicate more and longer-duration compound flood events in site 2. Oulu than would be expected based on the climatic conditions and neighbouring sites. In this site, the discharge station is located at the river mouth, only three kilometres from the mareograph, while in most sites the discharge data come from stations tens of kilometres upstream. This study setting potentially causes that the discharge observations (calculated with a rating curve from river water level) to some extent reflect sea level variation, which may lead to an overestimation of the co-variability of sea level and discharge.

We find it important for our understanding to examine compound flooding as a separate process from the long-term sea level trend. However, the society would benefit from transforming the identified compound flood hazards to the fixed national datum. In a geographical setting like Finland, that is experiencing relative sea level decline, this examination would show that the increasing compound flood potential does not automatically increase the risk on housing and important infrastructure as their elevation relative to the mean sea level increases. It would also be interesting to compare the flood heights and duration of the most severe compound flood events to the flooding caused by annual spring snowmelt flooding in the northernmost sites in Finland and in other high-latitude coasts. Namely, because ecosystems and societies have adapted to regular spring flooding, floods that remain within these typical levels are unlikely to cause severe impacts, unless they disrupt seasonal activities on the floodplains. This type on study would, however, require considerable knowledge and data of the local environmental setting and local community.

5. Conclusions

Compound flood potential currently decreases with latitude in the Baltic Sea coasts of Finland, but also eastward from the Archipelago Sea (closest to the Baltic Proper) coast toward the Gulf of Finland coasts. These patterns may reflect the main latitudinal gradient in the seasonal streamflow variation, but also differences in the catchment and river channel characteristics, river regulation and location of the paired sea level and discharge stations. When explicitly separated from the sea level trend, the compound flood potential is not uniformly increasing. In the north (66° N), the compound flood potential is increasing, potentially due to shortening of the winter season. However, no consistent trend is found at 60° N: instead, there are substantial site-specific differences in how the compound potential is changing over time. For a better process understanding, we call for future studies that treat sea level trends and the co-variability of sea level and streamflow as separate phenomena, and are able to identify potential compound events outside the high-latitude streamflow peak season. We also highlight the value of studies that combine sea level and streamflow observations with actual estuarine water level measurements, enabling direct inference of estuary-scale processes.

Funding

This work was supported by the Research Council of Finland [grant number 359247] Flagship Programme funding for the Digital Waters Flagship (DIWA).

CRediT authorship contribution statement

Tua Nylén: Conceptualization, Data curation, Formal analysis, Methodology, Software, Validation, Visualization, Writing – original draft. **Harri Tolvanen**: Conceptualization, Validation, Writing – review and editing.

CRediT authorship contribution statement

Tua Nylén: Writing – original draft, Visualization, Validation, Software, Methodology, Formal analysis, Data curation, Conceptualization. **Harri Tolvanen:** Writing – review & editing, Validation, Conceptualization.

Declaration of Competing Interest

The authors declare the following financial interests/personal relationships which may be considered as potential competing interests: Tua Nylén reports financial support was provided by Research Council of Finland. If there are other authors, they declare that they have no known competing financial interests or personal relationships that could have appeared to influence the work reported in this paper.

Appendix A. Supplementary tables and figures

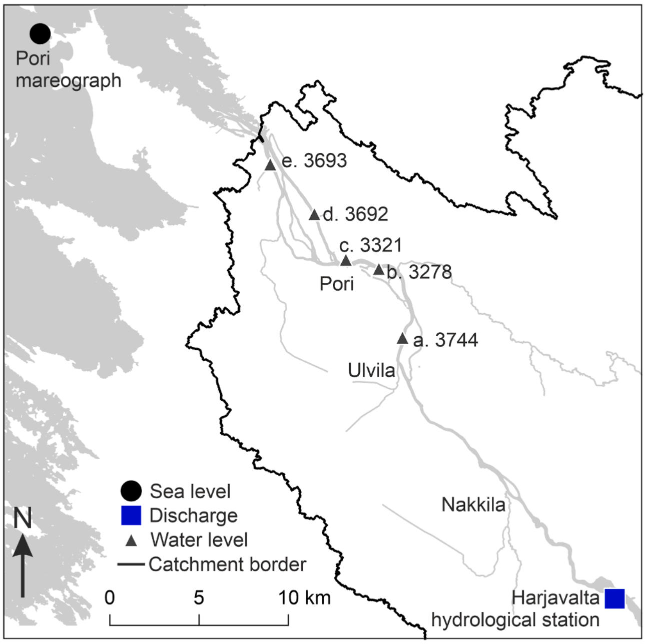

Figure A.1. Five water level stations a.–e. of the lower Kokemäenjoki river, describing actual water level variation between the Harjavalta hydrological station and Pori mareograph at site 6. Pori (Table 1)

Table A.1
Sea level linear trend slope and intercept, used and detrending sea level, and the spring snowmelt windows for the 11 sites along the coast of Finland

Site (River)	**Sea level linear trend slope** (mm per day)	**Intercept** (mm in Jan 1st 1970)	**Start**	**End**
1. Simo–Kemi (Simojoki)	-0.014	392	April 20th	June 13th
2. Oulu (Oulujoki)	-0.014	383	-	-
3. Kalajoki–Raahe (Kalajoki)	-0.015	395	April 7th	May 23rd
4. Pietarsaari (Esse å)	-0.015	391	April 7th	May 26th
5. Vaasa (Laihianjoki)	-0.016	391	March 29th	May 15th
6. Pori (Kokemäenjoki)	-0.011	346	April 3nd	May 15th
7. Rauma (Lapinjoki)	-0.010	328	March 29th	May 3rd
8. Turku (Aurajoki)	-0.007	275	March 26th	April 28th
9. Salo–Hanko (Uskelanjoki)	-0.003	246	March 25th	April 28th
10. Helsinki (Vantaanjoki)	-0.002	252	March 27th	May 7th
11. Kotka–Hamina (Kymijoki)	<0.001	243	April 1st	April 23rd

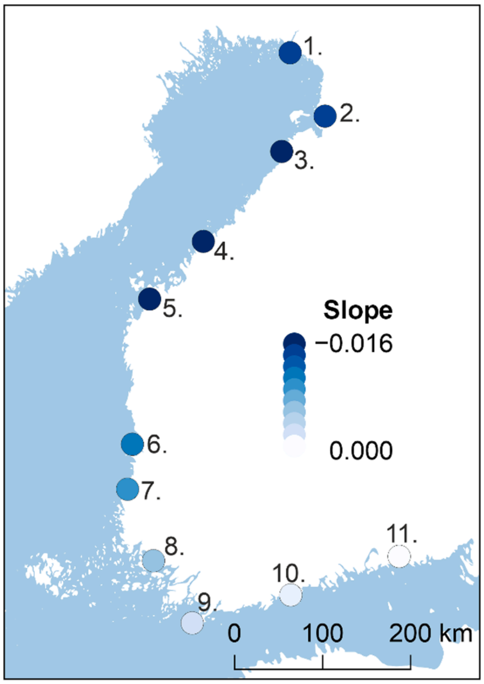

Figure A.2. The raw slope coefficient (in mm per day) of the linear sea level trend in the 11 Finnish mareographs in 1971–2024. See Table 1 for site descriptions and appendix Table A.1 for the numerical values

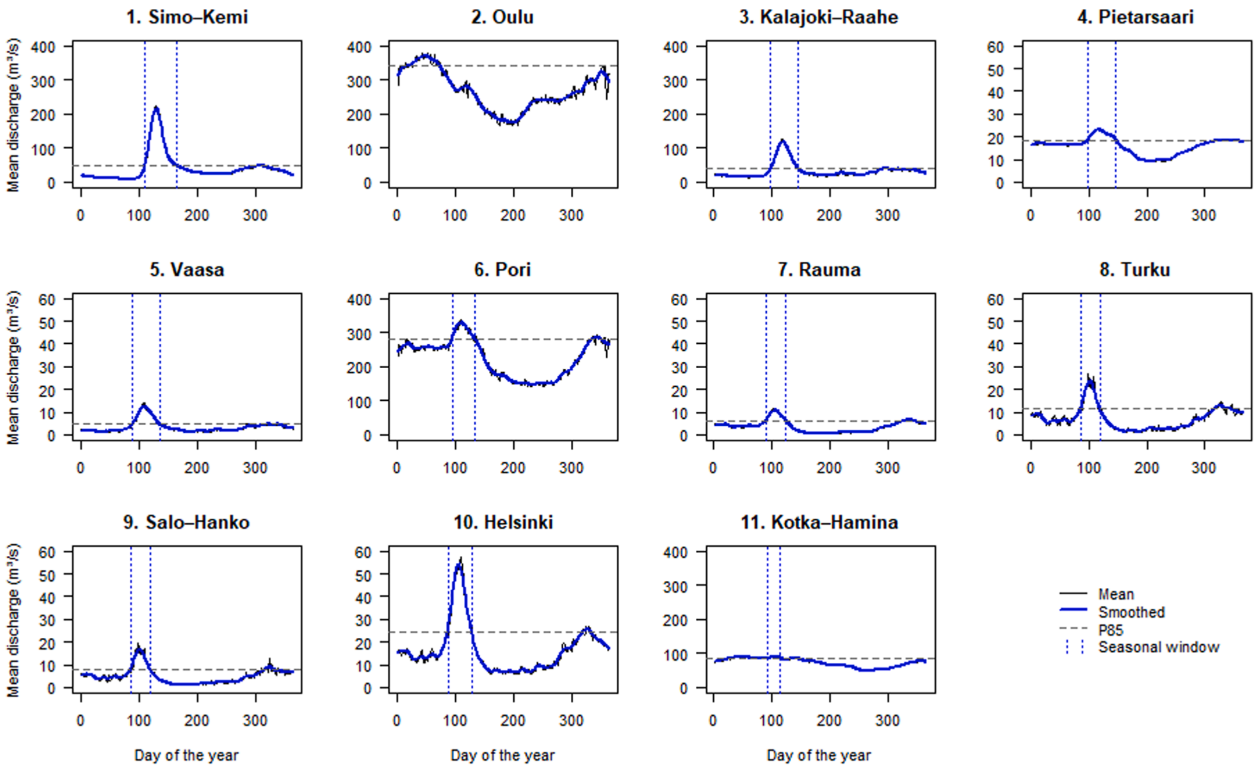

Figure A.3. Spring snowmelt seasonal windows excluded from the "seasonal" time-series. No window was found for site 2. Oulu (Oulujoki), as the highest discharges were measured during winter and autumn months. Note two different y-axis scales, for rivers with discharge observations below and above 60 m^3 /s

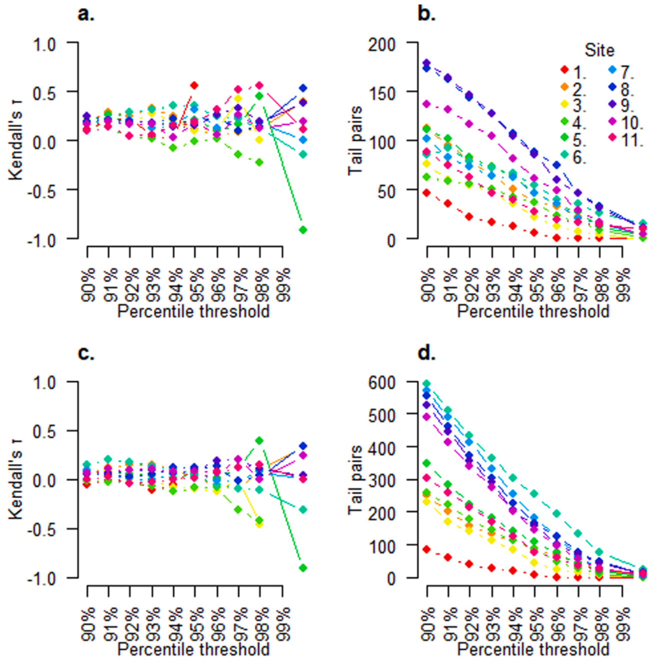

Figure A.4. Kendall's τ between the tail pairs of the event peak sea level and discharge (**a**), and the number of tail pairs (**b**) by selected percentile threshold in the 11 sites. For panels a–b, individual days with high sea level and discharge were aggregated into multi-day events separated by three days or less. The analysis was repeated for individual daily observations (**c–d**), resulting in similar general patterns

Table A.2
Goodness-of-fit of the Gumbel copula models of the high-tail (P_{90}) dependence, measured with a parametric bootstrapping-based test statistic and associated p-value. The results are reported for both the full dataset and the "seasonal" dataset excluding the spring snowmelt season. The p-value of the Gumbel copula for the full dataset is also compared to those of Clayton and Gauss copula models

	Full				Seasonal	
	Statistic	p-value			Statistic	p-value
Site	Gumbel	Gumbel	Clayton	Gauss	Gumbel	Gumbel
11. Simo–Kemi	0.031	0.308	< 0.001	0.113	0.024	0.362
2. Oulu	0.032	0.108	< 0.001	0.032	0.032	0.106
3. Kalajoki–Raahe	0.030	0.173	0.015	0.011	0.020	0.567
4. Pietarsaari	0.029	0.262	0.015	0.759	0.024	0.405
5. Vaasa	0.019	0.646	0.015	0.197	0.016	0.705
6. Pori	0.030	0.162	0.004	0.045	0.017	0.734
7. Rauma	0.024	0.322	0.175	0.385	0.027	0.198
8. Turku	0.020	0.480	0.046	0.396	0.027	0.169
9. Salo–Hanko	0.017	0.651	0.016	0.572	0.017	0.673
10. Helsinki	0.033	0.088	0.008	0.075	0.038	0.042
11. Kotka–Hamina	0.043	0.039	0.021	0.036	0.047	0.018

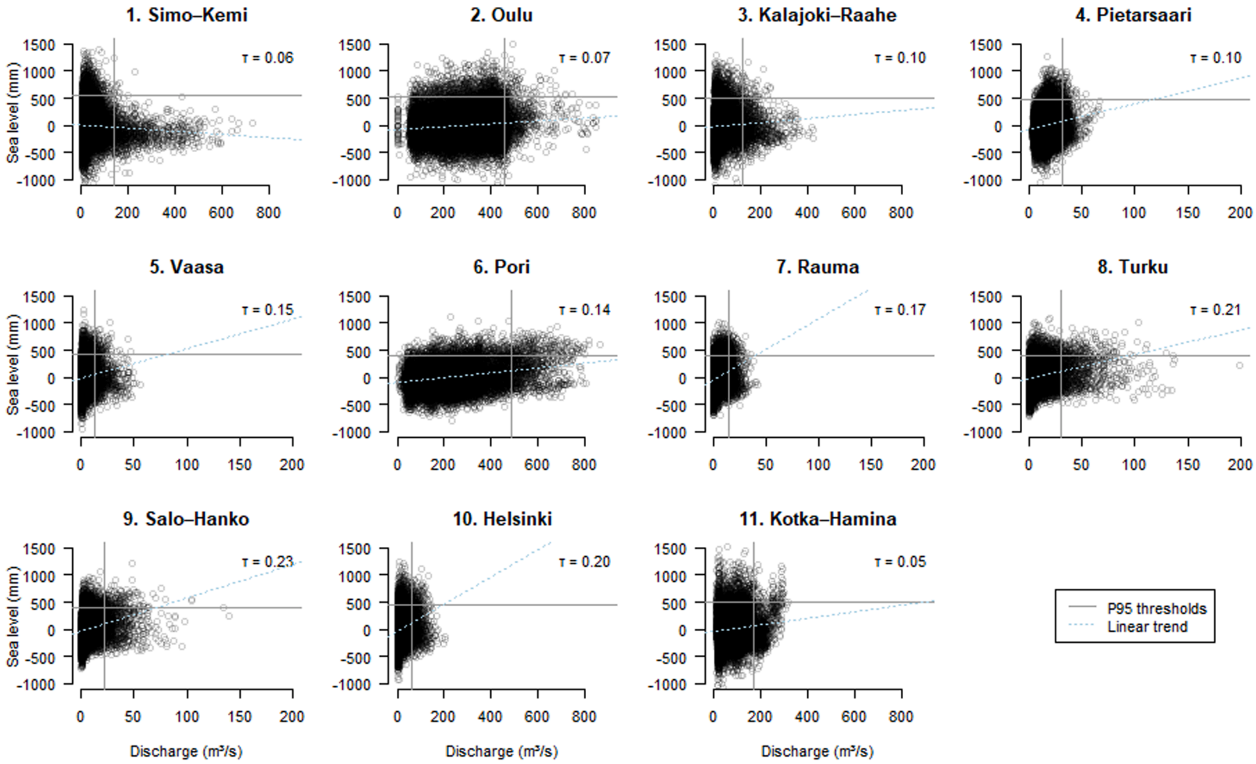

Figure A.5. Distribution of the daily (detrended) sea level and discharge observations at the 11 sites. Kendall's τ, P_{95} thresholds for sea level and discharge, and linear trend lines are also shown. Note two different x-axis scales, for rivers with discharge observations below and above 200 m^3 /s

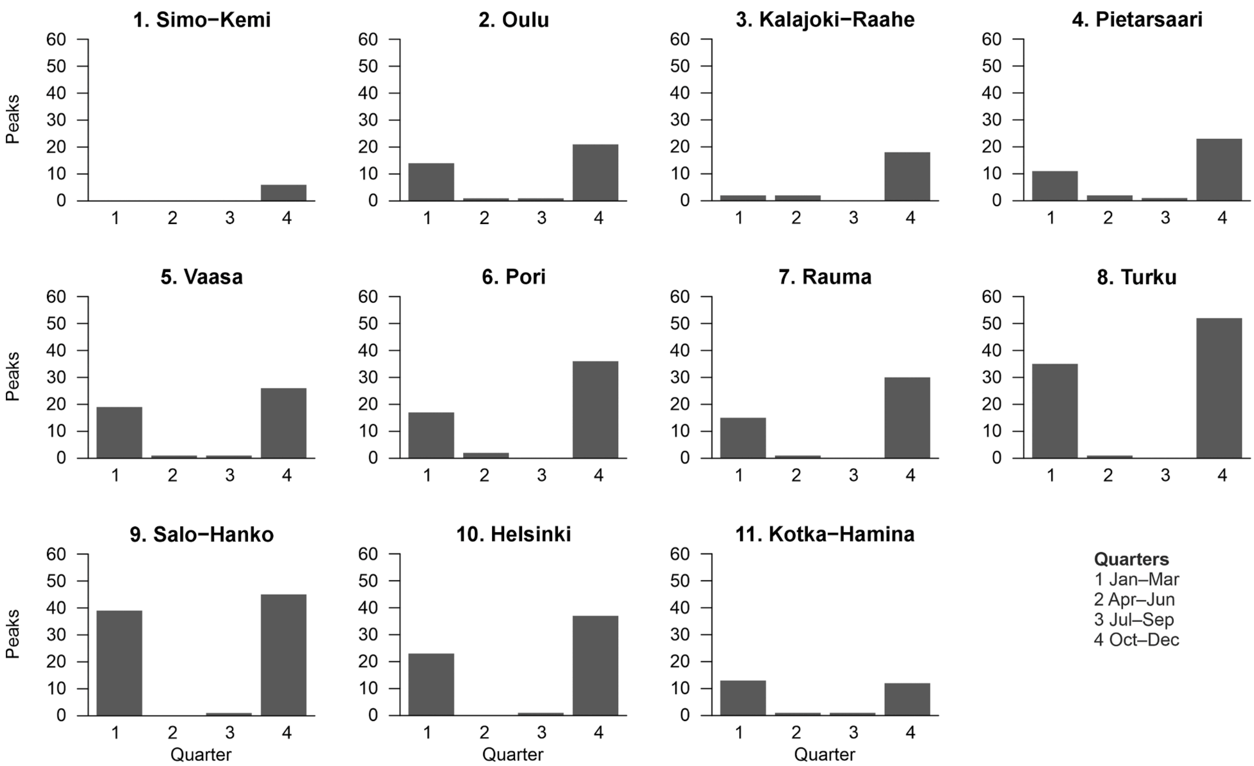

Figure A.6. Quarterly distribution of compound peaks calculated for the full year-round dataset

Appendix A. Supporting information

Supplementary data associated with this article can be found in the online version at doi: 10.1016/j.ejrh.2026.103551.

Data availability

All data examined in the study have been previously published open access. Code for statistical analyses is published as a supplement to this paper.

References

Baldan, D., Coraci, E., Crosato, F., Ferla, M., Bonometto, A., Morucci, S., 2022. Importance of non-stationary analysis for assessing extreme sea levels under sea level rise. Nat. Hazards Earth Syst. Sci. 22, 3663–3677. https://doi.org/10.5194/nhess-22-3663-2022.

Barbosa, S.M., 2008. Quantile trends in Baltic sea level. Geophys. Res. Lett. 35, L22704. https://doi.org/10.1029/2008GL035182.

Baumann, T.M., Polyakov, I.V., Pnyushkov, A.V., Rember, R., Ivanov, V.V., Alkire, M.B., Goszczko, I., Carmack, E.C., 2018. On the seasonal cycles observed at the continental slope of the eastern Eurasian Basin of the Arctic Ocean. J. Phys. Oceanogr. 48, 1451–1470. https://doi.org/10.1175/JPO-D-17-0163.1.

Bevacqua, E., Maraun, D., Hobæk Haff, I., Widmann, M., Vrac, M., 2017. Multivariate statistical modelling of compound events via pair-copula constructions: analysis of floods in Ravenna (Italy). Hydrol. Earth Syst. Sci. 21, 2701–2723. https://doi.org/10.5194/hess-21-2701-2017.

Bevacqua, E., Maraun, D., Vousdoukas, M.I., Voukouvalas, E., Vrac, M., Mentaschi, L., Widmann, M., 2019. Higher probability of compound flooding from precipitation and storm surge in Europe under anthropogenic climate change. Sci. Adv. 5, eaaw5531. https://doi.org/10.1126/sciadv.aaw5531.

Bevacqua, E., Vousdoukas, M.I., Zappa, G., Hodges, K., Shepherd, T.G., Maraun, D., Mentaschi, L., Feyen, L., 2020. More meteorological events that drive compound coastal flooding are projected under climate change. Commun. Earth Environ. 1, 47. https://doi.org/10.1038/S43247-020-00044-Z.

Bierstedt, S.E., Hünicke, B., Zorita, E., 2015. Variability of wind direction statistics of mean and extreme wind events over the Baltic Sea region. Tellus A Dyn. Meteorol. Oceanogr. 67, 29073. https://doi.org/10.3402/tellusa.v67.29073.

Bring, A., Fedorova, I., Dibike, Y., Hinzman, L., Mård, J., Mernild, S.H., Prowse, T., Semenova, O., Stuefer, S.L., Woo, M.-K., 2016. Arctic terrestrial hydrology: A synthesis of processes, regional effects, and research challenges. J. Geophys. Res. Biogeosciences 121, 621–649. https://doi.org/10.1002/2015JG003131.

Coles, S., 2001. An introduction to statistical modeling of extreme values. Springer, London, New York.

Couasnon, A., Sebastian, A., Morales-Nápoles, O., 2018. A copula-based Bayesian network for modeling compound flood hazard from riverine and coastal interactions at the catchment scale: an application to the Houston Ship Channel, Texas. Water 10, 1190. https://doi.org/10.3390/w10091190.

Couasnon, A., Eilander, D., Muis, S., Veldkamp, T.I.E., Haigh, I.D., Wahl, T., Winsemius, H.C., Ward, P.J., 2020. Measuring compound flood potential from river discharge and storm surge extremes at the global scale. Nat. Hazards Earth Syst. Sci. 20, 489–504. https://doi.org/10.5194/nhess-20-489-2020.

van der Wahl, W., Braun, A., Wu, P., Sideris, M.G., 2009. Prediction of decadal slope changes in Canada by glacial isostatic adjustment modelling. Can. J. Earth Sci. 46, 587–595. https://doi.org/10.1139/E09-044.

Ekman, M., Mäkinen, J., 1996. Recent postglacial rebound, gravity change and mantle flow in Fennoscandia. Geophys. J. Int. 126, 229–234. https://doi.org/10.1111/j.1365-246X.1996.tb05281.x.

Fang, J., Wahl, T., Fang, J., Sun, X., Kong, F., Liu, M., 2021. Compound flood potential from storm surge and heavy precipitation in coastal China: dependence, drivers, and impacts. Hydrol. Earth Syst. Sci. 25, 4403–4416. https://doi.org/10.5194/hess-25-4403-2021.

Fassert, C., November, V., Rey-Thibault, C., 2023. Facing nonscalability: are risks still 'risks' when compound and catastrophic? J. Risk Res. https://doi.org/10.1080/13669877.2023.2259414.

Fernández-Montblanc, T., Gómez-Enri, J., Ciavola, P., 2020. The role of mean sea level annual cycle on extreme water levels along European coastline. Remote Sens. 12, 3419. https://doi.org/10.3390/rs12203419.

Finnish Environment Institute, 2025. Hydrologiarajapinta. ⟨https://rajapinnat.ymparisto.fi/api/Hydrologiarajapinta/1.1/⟩ (accessed 27 December 2025).

Finnish Environment Institute, 2026. Hydrologiset havaintopaikat [in Finnish, "Hydrological stations"]. ⟨https://ckan.ymparisto.fi/dataset/hydrologiset-havaintopaikat⟩ (accessed 6 April 2026).

Finnish Meteorological Institute, 2025a. Guidance to open data observations. ⟨https://en.ilmatieteenlaitos.fi/guidance-to-observations⟩ (accessed 27 December 2025).

Finnish Meteorological Institute, 2025b. FMI Open data WFS services. ⟨https://en.ilmatieteenlaitos.fi/open-data-manual-fmi-wfs-services?doAsUserLanguageId=en_US⟩ (accessed 27 December 2025).

Finnish Meteorological Institute, 2025c. Mareographs measure water level. ⟨https://en.ilmatieteenlaitos.fi/mareograph⟩ (accessed 6 April 2026).

Finnish Meteorological Institute, 2026. Warnings on the sea water level. ⟨https://en.ilmatieteenlaitos.fi/warnings-on-the-sea-water-level⟩ (accessed 6 April 2026).

Ganguli, P., Paprotny, D., Hasan, M., Güntner, A., Merz, B., 2020. Projected changes in compound flood hazard from riverine and coastal floods in northwestern Europe. Earth's. Future 8, e2020EF001752. https://doi.org/10.1029/2020EF001752.

Ghanbari, M., Arabi, M., Kao, S.-C., Obeysekera, J., Sweet, W., 2021. Climate change and changes in compound coastal–riverine flooding hazard along the U.S. coasts. Earth'S. Future 9, e2021EF002055. https://doi.org/10.1029/2021EF002055.

Green, J., Haigh, I.D., Quinn, N., Neal, J., Wahl, T., Wood, M., Eilander, D., de Ruiter, M., Ward, P., Camus, P., 2025. Review article: a comprehensive review of compound flooding literature with a focus on coastal and estuarine regions. Nat. Hazards Earth Syst. Sci. 25, 747–816. https://doi.org/10.5194/nhess-25-747-2025.

Hao, Z., Singh, V., Hao, F., 2018. Compound extremes in hydroclimatology: a review. Water 10, 718. https://doi.org/10.3390/w10060718.

Heinrich, P., Hagemann, S., Weisse, R., Gaslikova, L., 2023. Changes in compound flood event frequency in northern and central Europe under climate change. Front. Clim. 5, 1227613. https://doi.org/10.3389/fclim.2023.1227613.

Hinkel, J., Lincke, D., Vafeidis, A.T., Perrette, M., Nicholls, R.J., Tol, R.S.J., Marzeion, B., Fettweis, X., Ionescu, C., Levermann, A., 2014. Coastal flood damage and adaptation costs under 21st century sea-level rise. Proc. Natl. Acad. Sci. USA 111 (9), 3292–3297. https://doi.org/10.1073/pnas.1222469111.

Hofert, M., Kojadinovic, I., Maechler, M., Yan, J., 2024. copula: multivariate dependence with copulas. R. Package Version 1, 1–4. ⟨https://CRAN.R-project.org/package=copula⟩ (accessed 27 December 2025).

Ikeuchi, H., Hirabayashi, Y., Yamazaki, D., Muis, S., Ward, P.J., Winsemius, H.C., Verlaan, M., Kanae, S., 2017. Compound simulation of fluvial floods and storm surges in a global coupled river–coast flood model: model development and its application to 2007 Cyclone Sidr in Bangladesh. J. Adv. Model. Earth Syst. 9, 1847–1862. https://doi.org/10.1002/2017MS000943.

Jin, Y., Chen, M., Yan, H., Wang, T., Yang, J., 2023. Sea level variation in the Arctic Ocean since 1979 based on ORAS5 data. Front. Mar. Sci. 10, 1197456. https://doi.org/10.3389/fmars.2023.1197456.

Johansson, M., Boman, H., Kahma, K.K., Launiainen, J., 2001. Trends in sea level variability in the Baltic Sea. Boreal Environ. Res. 6, 159–179. ⟨https://www.borenv.net/BER/archive/pdfs/ber6/ber6-159s.pdf⟩ (accessed 29 December 2025).

Karabil, S., Zorita, E., Hünicke, B., 2017. Mechanisms of variability in decadal sea-level trends in the Baltic Sea over the 20th century. Earth Syst. Dyn. 8, 1031–1046. https://doi.org/10.5194/esd-8-1031-2017.

Kupfer, S., Vafeidis, A.T., MacPherson, L.R., 2025. Accounting for compound flooding can prevent maladaptation—A Baltic Sea case study. Earth's. Future 13, e2024EF005106. https://doi.org/10.1029/2024EF005106.

Lai, Y., Li, Q., Li, J., Zhou, Q., Zhang, X., Wu, G., 2021. Evolution of frequency and intensity of concurrent heavy precipitation and storm surge at the global scale: implications for compound floods. Front. Earth Sci. 9, 660359. https://doi.org/10.3389/feart.2021.660359.

Lewis, M., Moftakhari, H., Passalacqua, P., 2024. Challenges for compound coastal flood risk management in a warming climate: a case study of the Gulf Coast of the United States. Front. Water 6, 1405603. https://doi.org/10.3389/frwa.2024.1405603.

Lidberg, M., Johansson, J.M., Scherneck, H.-G., Davis, J.L., 2007. An improved and extended GPS-derived 3D velocity field of the glacial isostatic adjustment (GIA) in Fennoscandia. J. Geod. 81, 213–230. https://doi.org/10.1007/s00190-006-0102-4.

Lintunen, K., Kasvi, E., Uvo, C.B., Alho, P., 2024. Changes in the discharge regime of Finnish rivers. J. Hydrol. Reg. Stud. 53, 101749. https://doi.org/10.1016/j.ejrh.2024.101749.

Little, A.S., Priestley, M.D.K., Catto, J.L., 2023. Future increased risk from extratropical windstorms in northern Europe. Nat. Commun. 14, 4434. https://doi.org/10.1038/s41467-023-40102-6.

Luxford, F., Faulkner, D., 2020. Recommendations for future research and practice on non-stationarity in UK flooding. FRS18087/REA/R2. Environment Agency, Bristol. ⟨https://assets.publishing.service.gov.uk/media/6038f813e90e07055685020c/Recommendations_for_future_research_and_practice_on_non-stationarity_in_UK_flooding_-_report_2_.pdf⟩ (accessed 27 December 2025).

Lyddon, C., Robins, P., Lewis, M., Barkwith, A., Vasilopoulos, G., Haigh, I., Coulthard, T., 2023. Historic spatial patterns of storm-driven compound events in UK estuaries. Estuaries Coasts 46, 30–56. https://doi.org/10.1007/s12237-022-01115-4.

McKeon, K., Piecuch, C.G., 2025. Compound minor floods and the role of discharge in the Delaware River Estuary. J. Geophys. Res. Oceans 130, e2024JC021716. https://doi.org/10.1029/2024JC021716.

Mishra, A., Mukherjee, S., Merz, B., Singh, V.P., Wright, D.B., Villarini, G., Paul, S., Kumar, D.N., Khedun, C.P., Niyogi, D., Schumann, G., Stedinger, J.R., 2022. An overview of flood concepts, challenges, and future directions. J. Hydrol. Eng. 27, 03122001. https://doi.org/10.1061/(ASCE)HE.1943-5584.0002164.

Moftakhari, H., Schubert, J.E., AghaKouchak, A., Matthew, R., Sanders, B.F., 2019. Linking statistical and hydrodynamic modeling for compound flood hazard assessment in tidal channels and estuaries. Adv. Water Resour. 128, 28–38. https://doi.org/10.1016/j.advwatres.2019.04.009.

Nasr, A., Wahl, T., Rashid, M.M., Camus, P., Haigh, I.D., 2021. Assessing the dependence structure between oceanographic, fluvial, and pluvial flooding drivers along the United States coastline. Hydrol. Earth Syst. Sci. 25, 6203–6227. https://doi.org/10.5194/hess-25-6203-2021.

Nicholls, R.J., Lincke, D., Hinkel, J., et al., 2021. A global analysis of subsidence, relative sea-level change and coastal flood exposure. Nat. Clim. Change 11, 338–342. https://doi.org/10.1038/s41558-021-00993-z.

Omstedt, A., Pettersen, C., Rodhe, J., Winsor, P., 2004. Baltic Sea climate: 200 yr of data on air temperature, sea level variation, ice cover, and atmospheric circulation. Clim. Res. 25, 205–216. https://doi.org/10.3354/cr025205.

Pavlov, V.K., 2001. Seasonal and long-term sea level variability in the marginal seas of the Arctic Ocean. Polar Res. 20, 125–248 https://doi.org/10.1111%2Fj.1751-8369.2001.tb00051.x.

Pellikka, H., Johansson, M.M., Nordman, M., Ruosteenoja, K., 2023. Probabilistic projections and past trends of sea level rise in Finland. Nat. Hazards Earth Syst. Sci. 23, 1613–1630. https://doi.org/10.5194/nhess-23-1613-2023.

Pfaff, B., McNeil, A., 2018. evir: Extreme values in R. R package version 1.7-4. ⟨https://CRAN.R-project.org/package=evir⟩ (accessed 27 December 2025).

R Core Team, 2024. R: A language and environment for statistical computing. R Foundation for Statistical Computing, Vienna, Austria. ⟨https://www.R-project.org/⟩ (accessed 27 December 2025).

Rentschler, J., Salhab, M., Jafino, B.A., 2022. Flood exposure and poverty in 188 countries. Nat. Commun. 13, 3527. https://doi.org/10.1038/s41467-022-30727-4.

de Ruiter, M.C., Couasnon, A., van den Homberg, M.J.C., et al., 2020. Why we can no longer ignore consecutive disasters. Earth`S. Future 8, e2019EF001425. https://doi.org/10.1029/2019EF001425.

Sangsefidi, Y., Bagheri, K., Davani, H., Merrifield, M., 2023. Data analysis and integrated modeling of compound flooding impacts on coastal drainage infrastructure under a changing climate. J. Hydrol. 616, 128823. https://doi.org/10.1016/j.jhydrol.2022.128823.

Sebastian, A., 2022. Compound flooding. In: Brody, S., Lee, Y., Kothuis, B.B. (Eds.), Coastal flood risk reduction - The Netherlands and the U.S. Upper Texas Coast. Elsevier, pp. 77–88. https://doi.org/10.1016/B978-0-323-85251-7.00007-X.

Seneviratne, S.I., Nicholls, N., Easterling, D., Goodess, C.M., Kanae, S., Kossin, J., Luo, Y., Marengo, J., McInnes, K., Rahimi, M., Reichstein, M., Sorteberg, A., Vera, C., Zhang, X., Rusticucci, M., Semenov, V., Alexander, L.V., Allen, S., Benito, G., Cavazos, T., Clague, J., Conway, D., Della-Marta, P.M., Gerber, M., Gong, S., Goswami, B.N., Hemer, M., Huggel, C., van den Hurk, B., Kharin, V.V., Kitoh, A., Tank, A.M.G.K., Li, G., Mason, S., McGuire, W., van Oldenborgh, G.J., Orlowsky, B., Smith, S., Thiaw, W., Velegrakis, A., Yiou, P., Zhang, T., Zhou, T., Zwiers, F.W., 2012. Changes in climate extremes and their impacts on the natural physical environment. In: Field, C.B., Barros, V., Stocker, T.F., Dahe, Q. (Eds.), Managing the risks of extreme events and disasters to advance climate change adaptation. Cambridge University Press, Cambridge, pp. 109–230.

Serafin, K.A., Ruggiero, P., Parker, K., Hill, D.F., 2019. What's streamflow got to do with it? A probabilistic simulation of competing oceanographic and fluvial processes driving extreme along-river water levels. Nat. Hazards Earth Syst. Sci. 19, 1415–1431. https://doi.org/10.5194/nhess-19-1415-2019.

Stephens, S., Bell, R.G., Haigh, I.D., 2020. Spatial and temporal analysis of extreme storm-tide and skew-surge events around the coastline of New Zealand. Nat. Hazards Earth Syst. Sci. 20, 783–796. https://doi.org/10.5194/nhess-20-783-2020.

Taherkhani, M., Vitousek, S., Barnard, P.L., Frazer, N., Anderson, T.R., Fletcher, C.H., 2020. Sea-level rise exponentially increases coastal flood frequency. Sci. Rep. 10, 6466. https://doi.org/10.1038/s41598-020-62188-4.

Tilloy, A., Malamud, B.D., Winter, H., Joly-Laugel, A., 2019. A review of quantification methodologies for multi-hazard interrelationships. Earth-Sci. Rev. 196, 102881. https://doi.org/10.1016/j.earscirev.2019.102881.

Vousdoukas, M.I., Mentaschi, L., Voukouvalas, E., Verlaan, M., Jevrejeva, S., Jackson, L.P., Feyen, L., 2018. Global probabilistic projections of extreme sea levels show intensification of coastal flood hazard. Nat. Commun. 9, 2360. https://doi.org/10.1038/s41467-018-04692-w.

Wahl, T., Jain, S., Bender, J., Meyers, S.D., Luther, M.E., 2015. Increasing risk of compound flooding from storm surge and rainfall for major US cities. Nat. Clim. Change 5, 1093–1097. https://doi.org/10.1038/nclimate2736.

Ward, P.J., Couasnon, A., Eilander, D., Haigh, I.D., Hendry, A., Muis, S., Veldkamp, T.I.E., Winsemius, H.C., Wahl, T., 2018. Dependence between high sea level and high river discharge increases flood hazard in global deltas and estuaries. Environ. Res. Lett. 13, 084012. https://doi.org/10.1088/1748-9326/aad400.

Ward, P.J., Daniell, J., Duncan, M., Dunne, A., Hananel, C., Hochrainer-Stigler, S., Tijssen, A., Torresan, S., Ciurean, R., Gill, J.C., Sillmann, J., Couasnon, A., Koks, E., Padrón-Fumero, N., Tatman, S., Tronstad Lund, M., Adesiyun, A., Aerts, J.C.J.H., Alabaster, A., Bulder, B., Campillo Torres, C., Critto, A., Hernández-Martín, R., Machado, M., Mysiak, J., Orth, R., Palomino Antolín, I., Petrescu, E.-C., Reichstein, M., Tiggeloven, T., Van Loon, A.F., Vuong Pham, H., de Ruiter, M.C., 2022. Invited perspectives: a research agenda towards disaster risk management pathways in multi-(hazard-)risk assessment. Nat. Hazards Earth Syst. Sci. 22, 1487–1497. https://doi.org/10.5194/nhess-22-1487-2022.

Waterinfo.fi, 2025. Finland's most accurate and up-to-date water information. ⟨https://www.vesi.fi/en/⟩ (accessed 17 December 2025).

Wickham, H., François, R., Henry, L., Müller, K., Vaughan, D., 2023. dplyr: A grammar of data manipulation. R package version 1.1.4. ⟨https://CRAN.R-project.org/package=dplyr⟩ (accessed 1 December 2025).

Wolski, T., Wiśniewski, B., 2020. Geographical diversity in the occurrence of extreme sea levels on the coasts of the Baltic Sea. J. Sea Res. 159, 101890. https://doi.org/10.1016/j.seares.2020.101890.

Wu, G., Liu, Q., Hang, X., Wang, J., 2024. Modelling the combined impact of sea-level rise, land subsidence, and tropical cyclones in compound flooding of coastal cities. Ocean & Coast. Manag. 234, 107107. https://doi.org/10.1016/j.ocecoaman.2024.107107.

Zakharchuk, E.A., Sukhachev, V.N., Tikhonova, N.A., Kouraev, A., Zakharova, E., 2022. Seasonal fluctuations in Baltic sea level determined from satellite altimetry. Cont. Shelf Res. 249, 104863. https://doi.org/10.1016/j.csr.2022.104863.

Zscheischler, J., Westra, S., van den Hurk, B.J.J.M., Seneviratne, S.I., Ward, P.J., Pitman, A., AghaKouchak, A., Bresch, D.N., Leonard, M., Wahl, T., Zhang, X., 2018. Future climate risk from compound events. Nat. Clim. Change 8, 469–477. https://doi.org/10.1038/s41558-018-0156-3.